Nucleation and growth of thin films of rod-like conjugated molecules

2013 J. Phys.: Condens. Matter 25 143202

(http://iopscience.iop.org/0953-8984/25/14/143202)

J. Phys.: Condens. Matter **25** (2013) 143202 (20pp) doi:10.1088/0953-8984/25/14/143202

TOPICAL REVIEW

Nucleation and growth of thin films of rod-like conjugated molecules

Gregor Hlawacek[1] **and Christian Teichert**[2]

[1] Physics of Interfaces and Nanomaterials, Institute for Nanotechnology, University of Twente, PO Box 217, 7500AE Enschede, The Netherlands
[2] Institute of Physics, Montanuniversitaet Leoben, Franz Josef Straße 18, A-8700 Leoben, Austria

E-mail: g.hlawacek@utwente.nl

Received 23 January 2013, in final form 14 February 2013
Published 11 March 2013
Online at stacks.iop.org/JPhysCM/25/143202

Abstract
Thin films formed from small molecules are rapidly gaining importance in different technological fields. To explain their growth, methods developed for zero-dimensional atoms as the film-forming particles are applied. However, in organic thin-film growth the dimensionality of the building blocks comes into play. Using the special case of the model molecule para-Sexiphenyl, we will emphasize the challenges that arise from the anisotropic and one-dimensional nature of building blocks. Differences or common features with other rod-like molecules will be discussed. The typical morphologies encountered for this group of molecules and the relevant growth modes will be investigated. Special attention is given to the transition between a flat-lying and upright orientation of the building blocks during nucleation. We will further discuss methods to control the molecular orientation and describe the involved diffusion processes qualitatively and quantitatively.

(Some figures may appear in colour only in the online journal)

Contents

1. Introduction

Research over the past decades on growth processes at an atomic scale has greatly enhanced our understanding of thin-film formation and crystal growth. In particular the realization that in addition to thermodynamic effects also kinetic limitations at the surface play an important role during the growth of thin films and crystals has helped to explain many growth phenomena [1–5]. Although a great level of understanding has been reached for many different processes, the vast majority of the systems contained single atoms as the film-forming entity. These are as such zero-dimensional particles.

A new class of thin-film materials—conjugated molecules (see figure 1 for examples)—has emerged in the past 20 years. As is demonstrated in figure 1, such molecules can be three-dimensional like tris(8-hydroxyquinoline)aluminum (Alq3), two-dimensional like the essentially planar Porphyrins and Phthalocyanines or one-dimensional like the Acences,

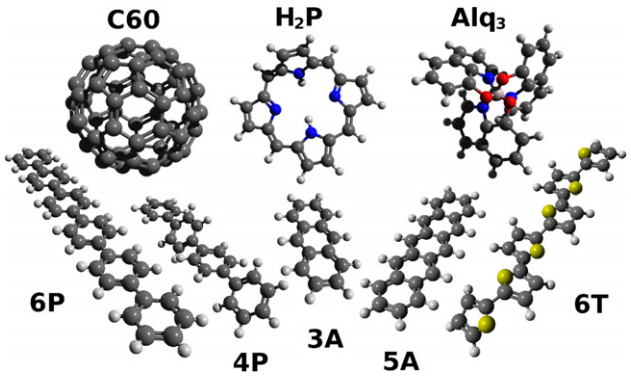

Figure 1. Examples of organic semiconductor molecules. In the first row the oligomers C_{60}, Porphyrin (H_2P), and Alq_3 (tris(8-hydroxyquinoline)aluminum) are shown. In the bottom row examples for some rod-like oligomers are presented. From left to right: para-Sexiphenyl (6P), para-Quaterphenyl (4P), Anthracene (3A), Pentacene (5A), and Sexitiophene (6T). Please note that while 4P is shown in the twisted gas phase configuration, 6P is depicted flat, as it is found in the bulk crystal structure.

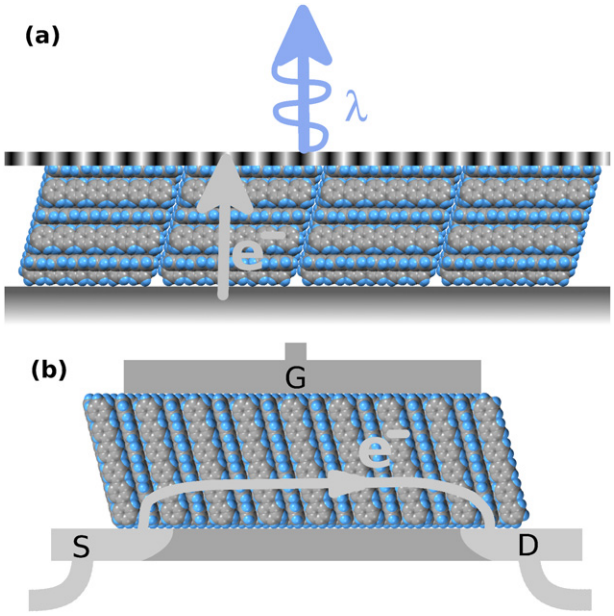

Figure 2. Schematic comparison of the required molecular orientations for device architectures based on rod-like conjugated molecules, using 6P as an example. (a) For OLED applications, the π-system should be oriented parallel to the substrate and the top electrode. For rod- or plate-like molecules, this usually requires a flat-lying configuration. (b) In an OTFT, the conjugated molecules should be oriented in an upright orientation. This facilitates an isotropic electric transport from source to drain parallel to the gate electrode. For holes, the requirements on molecular orientation are unchanged, as only the direction but not the path of the charge transport changes.

oligo-Phenylenes and Tiophenes. The spherical C_{60} molecule can either be viewed as a large zero-dimensional or a isotropic three-dimensional particle. Their use as organic semiconductors opens exiting new possibilities for electronic and optoelectronic devices, in particular flexible or stretchable [6] devices. There is ample evidence that models used in inorganic epitaxy might also be applicable to this new class of materials [7–9]. However, on a molecular level these materials do not always follow the well-established findings of classical epitaxy [10, 11]. In this topical review, the underlying reasons and consequences for thin-film growth will be discussed. A great variety of different conjugated molecules are currently under investigation and their number keeps steadily increasing. As many of the effects described here are thought to be generic, we will limit this topical review to rod-like molecules. They are a representative group within the vast number of molecules with extended dimensionality. In fact, we will restrict ourself mostly to the oligophenylene molecule para-Sexiphenyl (6P) [12–15]. This model molecule is widely investigated for its potential use in organic thin-film transistors (OTFT), organic light emitting diodes (OLED) and solar cells. In these devices, a specific molecular orientation is essential for optimal performance. By comparison to other rod-like molecules, we will highlight the modifications that arise in the growth behavior by changing molecular properties.

After a brief introduction to small organic molecules, first the nucleation behavior will be discussed. It is during this initial growth stage when the molecular orientation of the thin film is determined. This topic is of special importance as different applications require different molecular orientations on the substrate. The need to control this orientation is rooted in the anisotropic properties of the molecules. In particular, the charge carrier mobility for different crystallographic directions often shows a pronounced anisotropy [16, 17]. As a rule of thumb, charge transport is always best in directions with maximum π/π overlap. Often this is perpendicular to the long molecular axis or the molecular plane containing the conjugated π-system for two- and three-dimensional molecules. In figure 2, the required molecular orientations for a OTFT and an OLED are depicted for the model molecule 6P. As can be seen, the desired orientation for an OLED application would be flat-lying molecules with their π-systems parallel to the electrodes. Charge transport in such a device is then perpendicular to the π-system and the long molecular axis or largest plane. Also the desired light emission is maximized in such a configuration. On the other hand, for an OTFT application an upright standing molecular configuration is wanted to facilitate charge transport parallel to the substrate in an isotropic way. Therefore, possibilities to influence the nucleation behavior and, consequently, the resulting film morphology as well as the molecular orientation will be discussed.

Secondly, we will describe different growth modes and mechanisms observed during the formation of thicker films. Examples of Stranski–Krastanov and Volmer–Weber growth modes as well as Frank–van der Merwe or layer-by-layer (LbL) growth will be presented [1, 18]. Although difficult to achieve, the latter is often the desired growth mode to fabricate continuous films with homogeneous thickness. The so-obtained smooth interfaces have a lower number of defects and generally yield a higher charge carrier mobility [19–22]. Which of the above-mentioned thermodynamical growth modes is realized depends on the ratio of the different surface

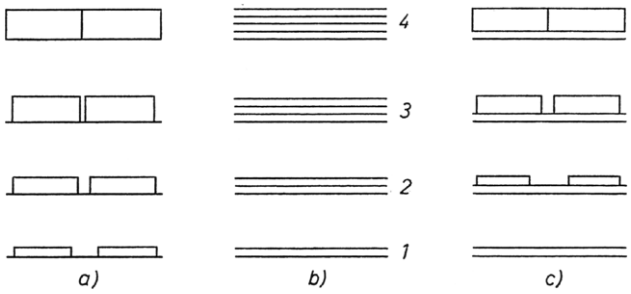

Figure 3. Schematic growth morphology for (*a*) Volmer–Weber, (*b*) Frank–van der Merwe, and (*c*) Stranski–Krastanov growth modes. Reprinted with permission from [18]. Copyright, © 1958 Oldenbourg Wissenschaftsverlag GmbH.

free energies. The following requirement has to be fulfilled for any thin-film growth to happen. The sum of the surface free energy σ_i between substrate and adsorbate, and σ between the adsorbate and the vapor are smaller than the surface free energy of the substrate σ_s [18]. Depending on the evolution of the change of the surface free energy

$$\Delta\sigma = \sigma + \sigma_i - \sigma_s \quad (1)$$

during deposition, the three growth modes presented in figure 3 can be distinguished. For $\Delta\sigma < 0$ at all times it is feasible for the substrate to be covered by the adsorbate layer. This growth mode is usually referred to as Frank–van der Merwe, layer-by-layer (LbL) or two-dimensional growth. If $\Delta\sigma > 0$ at all times clustering will occur. This mode is called Volmer–Weber, island or three-dimensional growth. If $\Delta\sigma < 0$ for the initial deposited layers but changes to $\Delta\sigma > 0$ for subsequently deposited material, the film will start to cluster after a thin uniform layer has been deposited. This growth mode is called Stranski–Krastanov growth mode. The latter is frequently found in inorganic heteroepitaxy for systems with a significant but not too large mismatch [23]. Unfortunately in organic thin-film growth, the last two growth modes are much more common than the desired LbL mode.

The above-sketched thermodynamic description of thin-film growth is not sufficient if the necessary diffusion processes are kinetically hindered. A more atomistic approach that includes the actual pathways is then needed to describe the observed morphologies accurately [24]. In particular, interlayer diffusion and the associated barriers play a decisive role. Ehrlich–Schwoebel or step edge barriers [25, 26], activation barriers for intralayer diffusion, and the anisotropy of these properties influence the final morphology. Depending on the absolute and relative sizes of these barriers, different morphologies will be found in the resulting thick films. As a result of the sizable step edge barrier often found in these molecular films, growth phenomena such as mound formation and rapid roughening are frequently observed. As the strong van der Waals interaction—typical for conjugated molecules—often dominates all other intermolecular and molecule–substrate interactions, three-dimensional growth is characteristic for organic semiconductor thin films.

For all the growth phenomena mentioned it is important to realize that already for one-dimensional molecules at least two different scenarios have to be distinguished. A smooth film grown in LbL mode might be useful for OLED applications when formed from flat-lying molecules. On the other hand, if the molecules have an upright orientation, already a small number of layers grown in LbL mode at the gate dielectric will yield a decent performance in an OTFT configuration. The reason that a small number of layers will suffice is related to the fact that all important charge transport processes are confined to the first 2 ML [27].

While many studies focus on the submonolayer regime and interpret the behavior of individual molecules, we follow a mesoscopic approach. This is justified by the fact that the behavior of larger ensembles of molecules allows one to infer information about the molecular level processes [1, 5]. In addition, the investigated mesoscopic size range correlates well with the final device dimensions. The relevance of different changes in the properties at this mesoscopic length scale can thus be directly related to the device performance.

1.1. Organic semiconductors

The conductivity of organic crystals had been studied already in the early 20th century [28, 29]. However, only with the discovery of electroluminescence did these materials receive additional attention from the semiconductor research community [30, 31]. Inspired by the Nobel prize awarded for the work of Heeger, Shirakawa, and MacDiarmid in the 1970s, many researchers focused on conjugated polymers, which exhibit good conductivity if prepared properly [32]. In the 1980s, organic heterojunctions [33] and organic thin-film transistors [34–36] were demonstrated. The final breakthrough happened after the realization of high-efficiency electroluminescence from organic light emitting diodes built both from polymers [37, 38] and oligomers [39, 40]. Nowadays, organic semiconductors are either already used or are about to enter the market soon in countless applications such as large-area lighting, flexible solar cells, and displays. These devices are based on the integrated use of OLEDs, OTFTs, sensors, and organic photovoltaic cells [41–45].

With respect to their growth behavior, organic semiconductors are of interest for several reasons. As described above, classic surface science treats zero-dimensional particles with a few exceptions such as Si dimers [46]. The extended shape of the used molecules not only allows them to adopt different orientations in space but also influences the way they interact with the surroundings. It is the extended electronic system that is responsible for the large intermolecular forces. The underlying van der Waals forces are small for the individual constituting atoms but can add up to a few eV for the entire molecule. The extended electronic system also helps to smoothen the effective corrugation of the substrate. The molecule averages over many possible atomic adsorption sites to find the molecular adsorption site with the minimum energy. Directly related to this is a large number of internal vibrational degrees of freedom [47, 48]. These have to be considered when discussing the interaction at interfaces. These interfaces can occur between the condensed phase and the 2D or 3D gas phase, but can also be boundaries between

different crystalline domains. Unfortunately, the large size of the building blocks results in a large number of translational domains. Together with the usually low symmetry of the crystal structure this can lead to additional disorder in the film, which in turn hampers the final device performance. For a general overview on the properties of organic semiconductors, the reader is referred to the following books [45, 49, 50].

1.2. Rod-like conjugated molecules

The three most important groups of rod-like conjugated molecules are the para-n-phenyls and the groups of acenes and thiophenes (see lower part of figure 1). The first two will be of particular interest here, as they show opposed properties in some important characteristics. The n-thiophene molecules are chiral and exhibit interesting chiral phenomena in thin layers but not in the bulk [51].

In this paper, we will focus primarily on para-Sexiphenyl (6P) [14, 52–54]. It is important to realize at this point that the acenes and para-n-phenyls have a very different stiffness of their backbone. The single bonds in the n-phenyls allow a certain flexibility of the backbone as compared to the acenes, which possess a much stiffer backbone formed by two bonds. In the case of the n-phenyls, the phenyl rings can twist with respect to each other (shown for 4P in figure 1). This twist is observed for single molecules either on the surface or in the gas phase. However, in a bulk crystal the n-phenyls adopt a flat configuration (as shown for 6P in figure 1) [15, 55]. Typically, rod-like molecules like the acenes or phenylenes form a so called herringbone bulk structure. This packing motif is characterized by an alternating left and right tilt of the molecular plane around the long molecular axis. As a result, the long hydrogen-terminated side of one molecule faces the flat side of the neighboring molecules where the π-system is located. This configuration balances the quadrupole moment of the molecules most effectively. It should be noted that this packing motif is very different from what is found for two-dimensional plate-like molecules, which favor a planar bulk stacking.

2. Forming a nucleus

In this section, the important quantity of interest is the so-called critical nucleus size i^*. It is defined as the largest number of particles forming a cluster that will become stable by adding one more particle. While there are various ways to extract this number, the use of rate theories [5] in combination with scanning probe techniques has been proved to be extremely successful. The central result of the underlying theory can be summarized by the relation

$$N \sim \left(\frac{F}{\nu}\right)^{\chi} \tag{2}$$

where N is the island number density, F denotes the flux of incoming particles in numbers of particles deposited per unit time and surface area. The scaling exponent $\chi = i^*/(i^* + 2)$ holds the dependence on the critical nucleus size.

$$\nu = \nu_0 \mathrm{e}^{-E_\mathrm{D}/(k_\mathrm{B}T)} \tag{3}$$

is the particle jump rate on the surface. Here, E_D is the energy barrier the particle has to overcome, T the temperature and k_B the Boltzmann factor. The pre-exponential factor $\nu_0 = 2k_\mathrm{B}T/h$ is often referred to as the attempt frequency. For all practical purposes, this is on the order of 10^{13} s^{-1} in inorganic systems. As we will see later, for organic systems ν_0 can deviate substantially from this value [48].

A second approach is based on the scaling hypothesis stating that the island statistics in the steady-state regime will depend—besides ν and F—only on the coverage Θ via the mean island size [56]. Using this assumption, it is possible to derive the critical nucleus size, although this is not very easy to apply in practice. This result has been extended by introducing an additional scaling for the capture numbers [57]. However, most often the empirical scaling function of Amar and Family [58] is used. Recently a similar approach has been introduced by Pimpinelli and Einstein, based not on the island size distribution but on the capture zone size distribution [59–61]. The presented scaling methods have the benefit that they require less data, and often a single experiment or even a single image can be sufficient to extract the critical nucleus size. A review and more in-depth analysis of the strong points and weaknesses of the individual methods can be found in [1, 2].

The above considerations are only valid for low coverages after the initial transient nucleation regime but before the coalescence occurs. This intermediate regime is called the steady-state nucleation regime.

An additional obstacle—for all three methods—results from the fact that the molecules are anisotropic. As a result they can adopt different in-plane orientations and out-of-plane orientations. As we will see later, the single shot methods also carry the risk of overlooking interesting kinetic behavior with respect to the deposition rate or growth temperature.

2.1. Obtaining the critical island size

In the case of complete condensation, i.e., when re-evaporation can be excluded, the island number density N can be written as [5]

$$N \propto \left(\frac{F}{\nu}\right)^{\chi} \mathrm{e}^{E_N/(k_\mathrm{B}T_\mathrm{D})}. \tag{4}$$

Here, T_D refers to the temperature of the sample during growth—often called the deposition temperature. The energy parameter

$$E_N = \frac{i^* E_\mathrm{D} + E_\mathrm{i}}{(i^* + 2)} \tag{5}$$

can be split further into the activation barrier for diffusion E_D and the binding energy of the critical nucleus E_i. Provided sufficient data is available, a plot of $\ln N$ versus $\ln F$ allows the extraction of the critical nucleus from the slope

$$\alpha_F = \chi = \frac{i^*}{i^* + 2}. \tag{6}$$

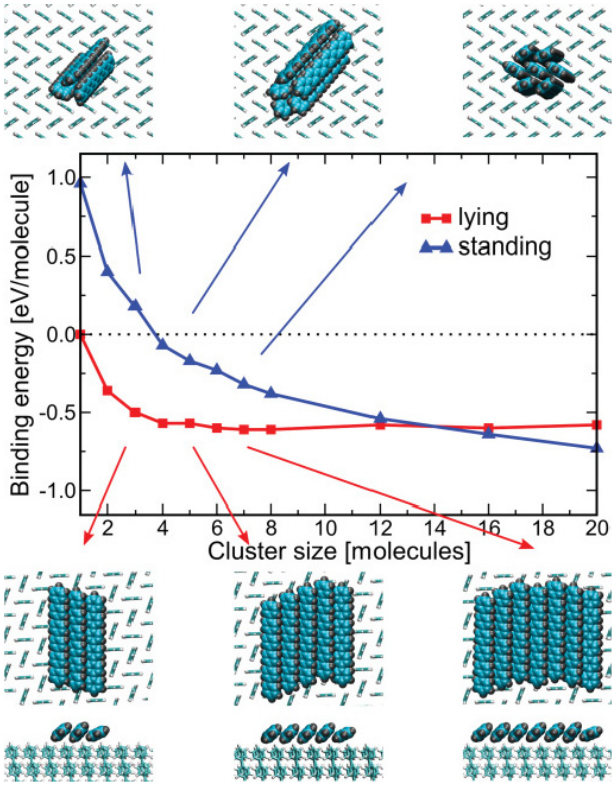

Figure 4. 6P cluster binding energy on a 6P(001) plane as function of cluster size. Graphs for clusters formed by upright standing and flat-lying molecules are presented. Snapshots of possible cluster geometries are shown for cluster sizes of 3, 5, and 7 molecules. While the top row shows the clusters formed from upright standing molecules, the corresponding clusters formed by flat-lying molecules can be found at the bottom. Please note that in the clusters formed by flat-lying molecules all molecules have their π-system exposed. In the seven-molecule cluster—and to a certain extent in the cluster formed by five standing molecules—some molecules have their π-system saturated [62]. Copyright (2011) by The American Physical Society.

Plotting the island density in an Arrhenius fashion as $\ln N$ versus $1/T_D$, one can extract again from the slope

$$\alpha_{TD} = \frac{i^* E_D + E_i}{(i^* + 2)k_B} \tag{7}$$

information on the involved energies. An assessment of the quality of the recorded data and the relevance of the extracted data can be obtained by comparing the results from the two different methods [5, 62]

$$y_{0F} + \alpha_F \ln F = y_{0T} + \frac{\alpha_{TD}}{T_D} \tag{8}$$

with y_{0R} and y_{0T} being the y-intercepts of the two above-mentioned plots.

The above-described approach based on the rate equation has been used extensively in the past to obtain information on the critical nucleus size. Typically sizes between 2 and 4 are found for different rod-like molecules. For 5A on SiO_2, a value of 3–4 is reported [9, 63], similar to 2–3 reported for 6P on disordered mica (0001) substrates [62]. However, due to the large experimental data set necessary, in many studies also scaling laws are used to determine the critical nucleus size. Most of the results are obtained by applying island size scaling [58]. However, capture zone scaling [59–61] seems to provide more reliable results [64–66] for some cases. In agreement with rate theory, scaling laws typically yield values between 2 and 3 for 6P [62, 64] and somewhat higher values between 3 and 6 for 5A [8, 9, 11] on SiO_2 or cyclohexane terminated Si{001} [67]. However, in particular for the growth of 5A, care has to be taken with respect to the applicability of these single shot methods because of fractal growth morphologies [68].

As will be demonstrated in the next section, the stability of the possible nuclei does not necessarily depend in a homologous way on the nucleus size. In fact, due to effective shielding some configurations can be more stable than others (see figure 5). 5A and 6P are very similar in regard to their herringbone packing in the bulk. Consequently, similar molecular configurations in the critical nucleus will have comparable stability with respect to other configurations.

As can be seen from (3), ν in (4) depends also on the attempt frequency ν_0. From the y-intercept y_{0T} in the above-mentioned Arrhenius plot, one can extract this quantity. It is important to note that for molecules this value does not always correspond to the one typically found in inorganic diffusion of zero-dimensional atoms ($\nu_0 = 1 \times 10^{13}$ s^{-1}). In fact, here the value of ν_0 can be much higher. Values up 5.6×10^{25} s^{-1} [69] are reported from thermal desorption spectroscopy (TDS). However, common values obtained from TDS (experimental and theoretical) are on the order of 1×10^{17} [47, 48, 69–74]. Recent rate equation analysis yields a value of 2×10^{17} for the diffusion of 6P on mica [62]. The explanation of these high values is given by transition state theory [75]. In this theory, the pre-exponential factor depends on the partition functions of the particle in the diffusive and adsorbed state. In contrast to an atom, a molecule possesses many vibrational and rotational degrees of freedom. In particular, the latter contribute only to the partition function of the diffusive state. As a result, the pre-exponential factor deviates from the well-known 1×10^{13} s^{-1}. The difference between values obtained by rate theory [62] and the sometimes extreme values obtained from TDS [69] arises from the different target phases. While in a typical growth experiment—used for the rate equation approach—the molecule stays on the surface in a 2D gas phase, in a TDS experiment the molecules enter the 3D vapor phase. However, the 3D phase has an even higher number of degrees of freedom compared to the 2D gas phase, resulting in different partition functions.

Independent of the above considerations, an interesting question concerning islands formed by upright molecules remains unsolved at the moment. How—and at what point during nucleation and growth—do the molecules reach an upright orientation? By considering the binding energy of an upright standing 6P molecule to the 6P(001) plane of 0.21 eV [159] and comparing it to the binding energy for a flat-lying molecule of 1.27 eV [76] it is plausible to assume that a single molecule will always take up a flat-lying configuration [77]. Eventually flat-lying molecules

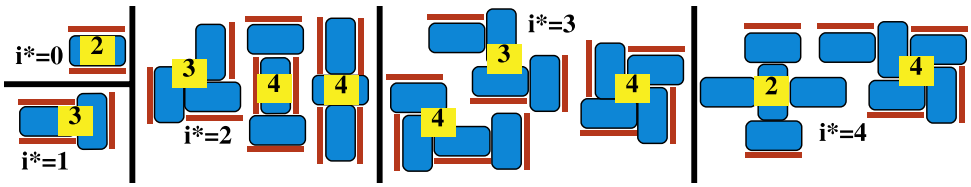

Figure 5. Illustration of some of the possible configurations of the critical nuclei for a rod-like molecule in an upright configuration. Assuming a herringbone-like configuration similar to the bulk structure, different possible nuclei configurations are sketched for $i^* = 0$ to 4. The yellow labels give the number of fully exposed π-systems (red bars). Configurations with one and five molecules yield a minimal number of fully exposed π-systems. Reprinted with permission from [78].

will meet and form initially unstable dimers and trimers that will decay or continue to grow and become stable when big enough. At some point—to form a film of upright standing molecules—the molecules have to change from a flat-lying to upright standing configuration. Recent molecular dynamics (MD) simulations illustrate the problem [62]. The graph presented in figure 4 shows the evolution of the cluster binding energy with increasing cluster size. The cluster binding energy is calculated by comparing a situation with i molecules in a cluster to the same number i of molecules adsorbed in a configuration lying on the 6P(001) surface. When the energy difference between the cluster and the separate molecules is negative, the cluster is thermodynamically stable. One can see that for $i < 4$ only flat-lying clusters are stable, while clusters formed from upright standing molecules are entirely unstable. For cluster sizes between 4 and 14 molecules, clusters of upright standing molecules are stable but flat-lying clusters would still be favored. Only for clusters larger than 14 molecules does 6P continue to grow in the required (001) orientation. However, the exact numbers will also depend on the details of the interaction with the substrate. In the MD simulation presented in figure 4, the clusters rested on the 6P(001) surface rather than on an amorphized mica substrate—discussed above—which is hard to simulate. In any case, the simulation results will be correct for second-layer nucleation as well as for all following layers.

More information can be extracted from the graphs shown in figure 4 on the growth of standing molecules. Already for clusters of only two molecules ($i^* = 1$) the energy gain is quite large (on the order of $10 \times kT$) and these clusters would be very stable. Furthermore, a simple geometric argument based on counting the number of fully exposed π-systems arrives at the same critical island size of $i^* \approx 3$–5 for upright standing molecules. This is also the value often reported in the literature [62–64]. In figure 5, several possible configurations of critical nuclei from $i^* = 0$ to 4 are sketched. The fully exposed π-systems are also marked and their number is given. A large number of exposed π-systems is energetically unfavorable, and the system would in general try to minimize their number. Besides the rough nature of the model it turns out that only for clusters of four ($i^* = 3$) or more molecules does the number of fully exposed π-systems become smaller than the number of molecules. From this simple model we can conclude that once the balance between molecules and exposed π-systems swings towards the molecules then the nuclei become stable. This is in good agreement with the above-presented MD results. The consequence of this can be seen twice in figure 4. First, the clusters formed by upright standing molecules become stable around a size which allows for molecules that do not belong to the island rim. Second, the final slope of the two graphs is different. With increasing cluster size the number of energetically more favorable molecules which are not part of the rim increases faster for clusters composed from upright standing molecules than for the flat-lying nuclei. At least for the investigated size range, clusters of flat-lying molecules contain only molecules which expose at least one π-system to the vacuum. Nucleation processes involving small metastable clusters (e.g. non-epitaxial dimers) that eventually convert into larger stable clusters are also observed in inorganic semiconductor epitaxy [79–81].

The important question is, how do these flat-lying molecules reach an upright standing orientation? Besides the reorientation of the whole cluster other scenarios are in principle possible as well. As we will see below, defects on the substrate surface influence the orientation of the molecules. First-principles calculations reveal that already a single defect in an otherwise perfect surface can alter the molecular orientation from flat-lying to upright standing [82]. The initial flat-lying nucleus can act in a similar way. Molecules arriving later will undergo a kind of defect nucleation and adopt an upright standing configuration. This is also observed in experiments. When the coexistence of structures formed from flat-lying and upright standing molecules is observed, the former are often responsible for nucleating the latter [83, 84].

Furthermore, already small clusters formed from upright standing nuclei should grow faster than their counterparts formed from flat-lying molecules. While molecules with all rotational orientations can be incorporated into a cluster of standing molecules, they will eventually have to rotate in the case of a cluster of flat-lying molecules. In any case, the calculation only yields the energetically most favorable configuration. It does not contain information on the probability that it can actually form. Thus, although energetically favorable, the flat-lying nuclei are actually more difficult to form due to the rotational hindrance. However, this implies that no substantial energy barrier exists for the reorientation of molecules from flat-lying to upright standing. Although no information is available on such a barrier, it cannot be too large, since the final morphology is dominated by upright standing molecules. Such a morphology would be unlikely in a scenario where initially both orientations

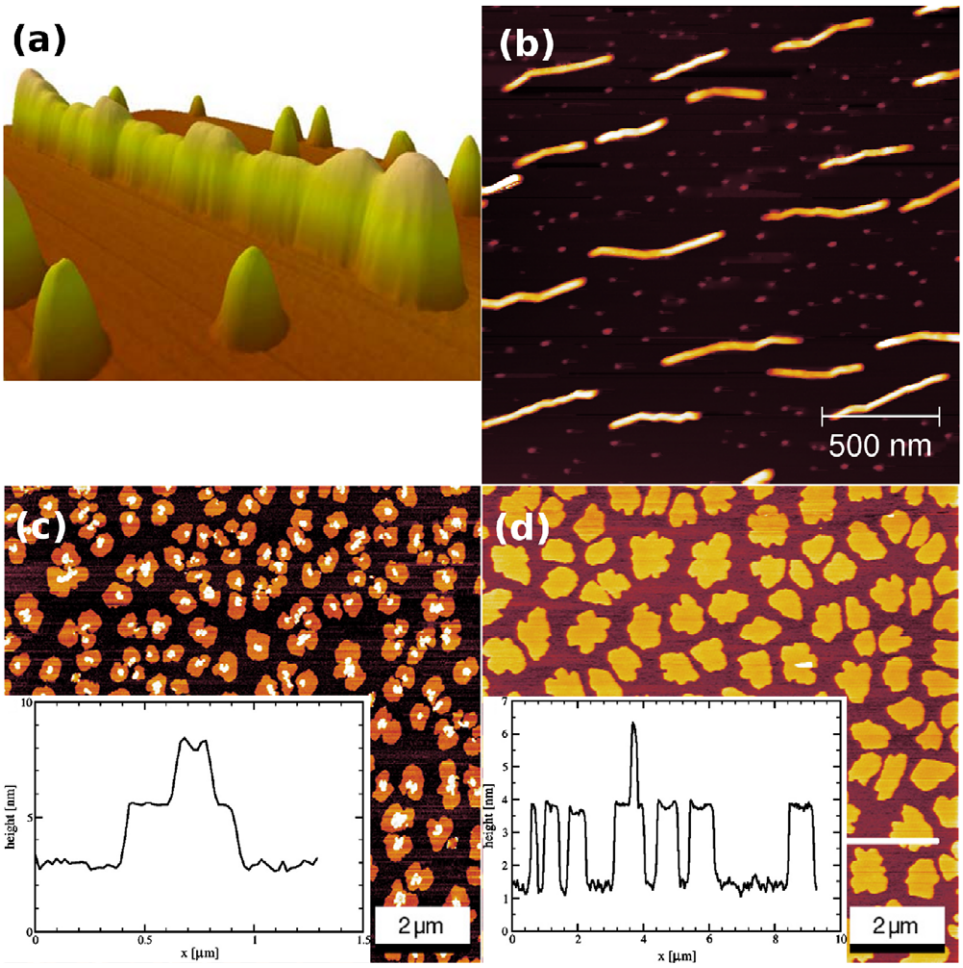

Figure 6. AFM analysis of 6P on mica: (a) 3D representation of a 850 nm long chain of 6P crystallites on mica. The film has been grown in 35 s at a substrate temperature of 360 K. (b) OMBE-grown 6P fibers on mica (0001). The film has a nominal thickness of 4 nm, and the sample temperature during growth was held at 360 K. The fibers consist of long segments. (c) 6P islands on carbon covered mica grown at 330 K (nominal film thickness 1 nm). (d) 6P islands on sputtered mica grown at 330 K (nominal film thickness 1 nm). The insets in ((c), (d)) are cross-sections revealing a terrace height of 2.6 nm, corresponding to the length of the molecule. (a) Reprinted from [88]. With kind permission from Springer Science and Business Media. (c), (d) Reprinted from [92]. Copyright (2007), with permission from Elsevier.

competed and a high barrier existed to obtaining the upright orientation. In such a competing scenario—where both types of nuclei can form—a cluster of upright molecules could be kinetically stabilized just because it can grow in size much more easily. Such an attachment-limited aggregation (ALA) for 6P has been observed and a critical nucleus size of $i^* = 7 \pm 2$ was found [85]. This is in reasonable agreement with the numbers obtained in the above simulations for the transition from unstable to stable for clusters formed by upright standing molecules. In such a scenario, no reconfiguration of the cluster from flat-lying to upright would be necessary.

2.2. Tuning the molecular orientation and the role of defects

Despite the persisting problems with respect to nucleation, several groups have succeeded in controlling the nucleation behavior. This is an important step towards the realization of functional devices, since different functionality requires different molecular orientations (see section 1 and figure 2).

A convenient, but technically not very practicable, method to control the molecular orientation is via the substrate. The observed changes in orientation go hand in hand with a change of the surface free energy of the substrate. Although the surface free energy is therefore the most obvious ordering parameter for the change from flat-lying to upright standing, we will use a different approach here. It is easy to see that the crystalline structure of the substrate surface plays a crucial role for the in-plane molecular orientation. However, the degree of order present in the substrate surface can also be decisive with respect to an upright or flat-lying molecular orientation. In fact, the effect of changing the surface structure can often dominate over the behavior expected from a substrate according to its other physical properties. A model system demonstrating this is the deposition of para-Sexiphenyl onto muscovite mica surfaces. Several groups have shown that for a large number of rod-like molecules—such as 6P, 5A, and 6T—nanofibers formed by flat-lying molecules are the dominant morphology on clean mica surfaces [54, 86–91].

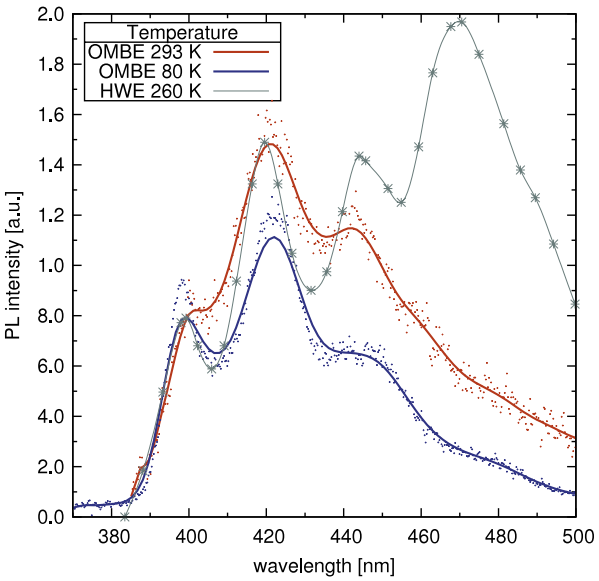

Figure 7. Steady-state photoluminescence of UHV OMBE-grown 6P fibers on mica (0001). The broad-band emission around 480 nm found in HWE grown fibers is missing. All curves are normalized to the 0–0 transition at 399 nm. PL measurements of OMBE-grown films courtesy of A Kadashchuk. (Data reproduced with permission from [95].)

In figure 6, typical morphologies obtained by atomic force microscopy (AFM) of 6P films grown on mica are presented. Figure 6(a) represents a particularly interesting case of nanofiber formation on mica (0001). Here, the spontaneous rearrangement of small crystallites on top of a wetting layer into chains of crystallites is observed [88]. We will discuss this interesting growth later in more detail. Changing the growth method from the used high-vacuum (HV) hot-wall epitaxy (HWE) to organic molecular beam epitaxy (OMBE) under ultra-high-vacuum (UHV) conditions does not influence the existence of a wetting layer. However, as can be seen from figure 6(b), this change in growth conditions results in the formation of larger, more uniform chain segments with a less pronounced internal structure [92–94]. The above-mentioned rearrangement process happens *in situ* during HWE growth.

The influence of the vacuum conditions can also be seen in photoluminescence (PL) spectra obtained from these anisotropic fibers (figure 7). In contrast to steady-state PL spectra obtained from HV HWE-grown 6P fibers [95], the broad-band emission around 480 nm is suppressed for UHV OMBE-grown fibers. The missing band at 480 nm can be connected to defect states resulting from structural defects. The absence of this band suggests a higher quality of the OMBE-grown films.

The important conclusion of the above observation is the following. HV conditions are usually sufficient to obtain reproducible and well-performing organic thin films. Given that the molecules are reasonable stable against oxidation and UV light, the obtained structures do not change over time in ambient conditions. However, the morphology (and the resulting properties) of organic thin films can easily be influenced by other small molecules. Results obtained under (U)HV conditions should be carefully reviewed with respect to their validity under ambient conditions. In particular, wetting layers and other possibly metastable structures far away from the bulk structure are sensitive to adsorbates.

Figures 6(c) and (d) show the result of two different approaches to reorient the molecules from flat-lying to upright standing. The molecules forming the crystallites and fibers in figures 6(a) and (b) have their long molecular axis parallel to the substrate. To obtain the morphology presented in figure 6(c), a surfactant[3]—namely carbon—has been predeposited on the clean mica (0001) surface. TDS has revealed that the full saturation coverage of surfactant completely suppresses the formation of a wetting layer [92]. In the presence of the surfactant, 6P films of upright standing molecules are formed. Similar experiments have been performed with 6P [69] and 4P [96–98] films on gold surfaces. In both cases, a reorientation of the molecules has been observed. It has to be pointed out that prior to the flat-lying/upright transition the epitaxy between the molecular film and the substrate is weakened. For the growth of 4P on Au{111} this is very well documented. On a clean Au{111} surface, the (211) contact plane of 4P has all molecules with their long axis parallel to the surface. Half of the molecules have their π-system parallel to the surface. After the addition of only 15% of a monolayer of carbon, the 4P contact plane changes to (201). The long axis of the molecules is still parallel to the substrate surface. However, in this 4P plane all molecules are tilted into an edge-on configuration, where the π-system is no longer fully facing the substrate. At the same time, the in-plane molecules loose their alignment with the substrate. After a further increase of the surfactant coverage to 0.5 ML, the molecules adopt an upright standing orientation. The new contact plane is the 4P(001). The weakened interaction with the substrate results in the formation of bent 4P nanofibers with a (201) contact plane on gold and, eventually, the formation of mounds composed of upright standing molecules [96, 97].

Finally, figure 6(d) also shows 6P islands on mica formed by upright standing molecules. However, this morphology has been achieved by breaking the surface symmetry of the substrate by ion bombardment of the substrate [92]. The nominal 1 nm thick film presented in figure 6(d) consists of islands formed by upright standing molecules, as is demonstrated by the cross section presented in the inset. The same reorientation can also be achieved by heating mica substrates to elevated temperatures [93]. More insight into the possible root cause for the reorientation on mica has recently been obtained using TDS. Putsche *et al* demonstrated recently that the existence of a wetting layer and the final orientation of the molecules is determined by the amount of potassium present on the surface [99]. The mechanism for the reorientation is similar to what has been shown above for a carbon pre-deposition.

Although similar experiments exist for other small conjugated molecules, the above series of experiments is

[3] The term surfactant is used here for a substance that influences the growth.

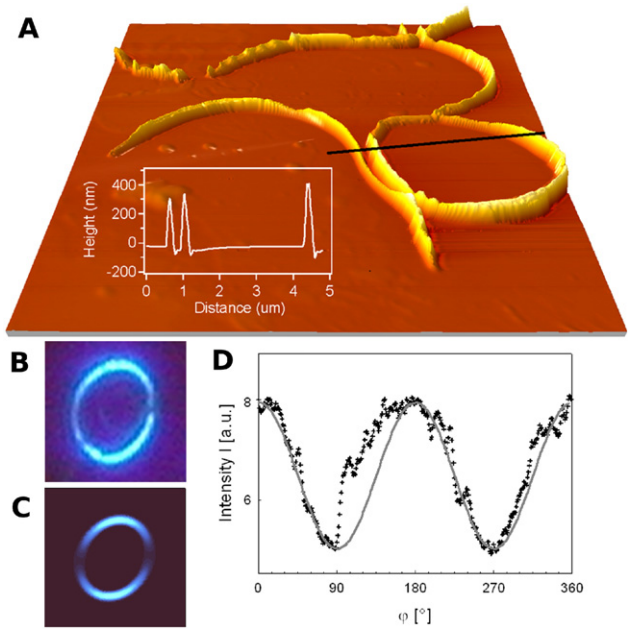

Figure 8. (A) AFM image (10 μm^2 $\times$ 10 μm^2) showing a 6P nanoring on pretreated mica. The inset presents the cross section along the indicated line. (B) Luminescence micrograph and (C) corresponding simulated image. In (D), the intensity along the rim (symbols) is plotted together with the one theoretically predicted according to Malus' law. Adapted with permission from [104]. Copyright (2003) American Chemical Society.

unique, as it clearly shows the importance for a well-ordered periodic substrate which can guide the molecules. The gradual loss of this guidance initially leads to an inferior quality of the crystals formed by flat-lying molecules. Finally, after significantly disturbing the surface order by surfactants or sputtering, the molecules choose to form films where their long molecular axis is perpendicular to the substrate surface. The loss of order in the substrate can be the result of a surfactant layer, sputtering, or the molecules themselves acting as *homosurfactants*. The latter is in particular true if the molecules are adsorbed on the substrate in a hit-and-stick mode. The initial molecules cannot align in an ordered manner and create a disordered substrate for the next layer [100, 101]. As expected from this discussion, using an amorphous substrate such as SiO_2 will lead to the formation of films formed by upright standing molecules [64, 102, 103]. However, often the layer of upright standing molecules itself can again act as a well-ordered substrate and can promote the successive growth of structures formed by flat-lying needles. See for example the needles forming on the 6P mounds grown on sputtered mica, as presented in figures 9(b) and (c) [76].

An extreme example of surfactant-mediated growth of nanofibers [104] is presented in figure 8. The mica surface has been pretreated with either water or methanol to remove the potassium atoms from the cleavage surface [105, 106]. It has been shown by AFM that the so created rings are several hundred nanometers high and have a typical diameter of 4 μm (see figure 8(A)). The luminescence micrograph presented in figure 8(B) and the corresponding simulation (figure 8(C)) reveal two things. First, the molecules lie flat on the surface and, second, their in-plane orientation rotates along the ring. As only molecules having their long axis parallel to the polarization of the incoming light yield maximum fluorescence, one observes a sinusoidal change in intensity along the ring (figure 8(D)) [104].

3. Diffusion and thin-film growth

In section 2 we have discussed the initial stages of film growth, i.e. the nucleation. After islands with a certain orientation have formed they need to grow, coalesce, and evolve into a complete film. Unfortunately, the asymmetric building blocks used often favor the formation of rough and anisotropic surface structures [76, 107–109]. Typically, one aims at a smooth film with a low number of grain boundaries and a flat surface. Grain boundaries represent inhomogeneities in the thin film and will have a negative effect on the transport properties [110–113]. On top of that they also affect the optical properties of the thin-film devices, such as nanofiber wave guides [104, 114–116]. Different growth techniques have been employed to achieve a smaller number of grain boundaries. Notably the use of thin organic layers [19] or self-assembled monolayers (SAM) [117] and

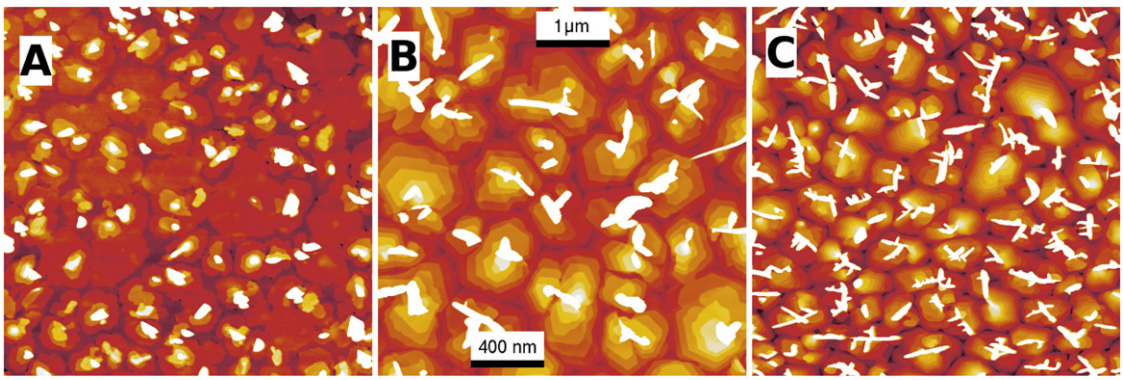

Figure 9. Para-Sexiphenyl mound formation on sputtered mica. The evolution of the film morphology with growing film thickness (4, 10, and 30 nm) can be seen. AFM image size: 5 μm; z-scale: 20, 35, and 50 nm. From [76]. Adapted with permission from AAAS.

supersonic molecular beam deposition (SuMBD) [118] allow one to influence the grain size without changing the substrate.

As has been discussed in the introduction, there can be severe deviations from the thermodynamic growth modes (figure 3) if the necessary diffusion mechanisms are kinetically hindered. The analysis of the morphology, and if necessary structural information, allows one to extract important physical quantities such as step edge barriers as well as parameters describing the growth mechanism. The generalized rules that can be deducted from the *in situ* and *ex situ* observations of film growth are valid for many molecules.

3.1. Mound formation

As we have discussed earlier, thin films of conjugated organic molecules which have their long axis perpendicular to the substrate are desired for OTFT-like applications. Although several approaches exist to achieve this desired orientation, the resulting films are often characterized by the formation of growth mounds due to rapid roughening [9, 11, 19, 108, 119, 120]. The resulting rough interface is undesired, as it negatively affects the charge carrier mobility [19–22]. Nevertheless, these rough films have been studied in the past as they allow interesting insights into molecular diffusion processes and thin-film growth mechanisms.

The process of rapid roughening is a result of an imbalance in the surface diffusion over step edges. If the downward particle flux over the step edge is dominant then the desired layer-by-layer growth mode is facilitated. However, in the case of a high step edge barrier for downward diffusion, which is described by a significant additional barrier—the so called Ehrlich–Schwoebel barrier (ESB) [25, 26]—mound formation will occur and rough morphologies will result. For the case of a very high ESB and realistic growth conditions, only atoms landing on the terrace $h-1$ will be incorporated into the terrace h. The coverage Θ of terrace h at time t for a given amount of deposited material $\bar{h} = Ft$ with the flux F can than be expressed by a Poisson distribution

$$\Theta_h(t) = 1 - \mathrm{e}^{-\bar{h}} \sum_{n=0}^{h-1} \frac{\bar{h}^n}{n!}. \tag{9}$$

Because $\Theta_1 = 1 - \mathrm{e}^{-\bar{h}}$ will always be smaller than 1, the first layer—and also all subsequent ones—never closes. As a result steep trenches are observed. Such Poisson-shaped mounds were already described in inorganic systems indirectly [121] and using real-space methods [122]. An in-depth theoretical analysis was conducted later by Elkinani and Villain, who used the ancient Greek Zeno Paradox to describe a peculiarity of the mound formation [123, 124]. In thin-film growth, the Zeno Paradox describes a situation where narrow trenches between mounds get so narrow that the probability for an atom or a molecule to land in the trench becomes increasingly smaller as the trench width decreases. After the unlikely event of a molecule entering the trench, the now narrower trench will have an even smaller probability to be filled by further molecules, and thus stays open. For this to be observable, a high step edge barrier has to prevent molecules landing on higher lying terraces from descending onto lower terraces deeper in the trench. As a result, the mounds get higher and higher but would never coalesce, thus the substrate would not be covered completely.

A detailed analysis of the involved atomic or molecular diffusion processes shows that in fact the time scales for the different basic processes play an important role [125]. First, there is the traversal time

$$\tau_{\mathrm{tr}} \approx A/\nu \tag{10}$$

a particle needs to visit all the sites on an island. Here, A corresponds to the size of the island (measured in lattice sites). The flux of incoming particles F determines the time

$$\Delta t = 1/(FA) \tag{11}$$

between the arrival of the particles forming the film. Finally, the residence time [125–128]

$$\tau = \frac{aL^2}{\nu} + \frac{bL}{\nu'} \tag{12}$$

describes the time a diffusing particle spends on an island with a characteristic size L (L is the island's circumference). Here, a and b are geometry-dependent constants. While the first term is on the order of the residence time (12), the second term accounts for the increase in residence time due to the step edge barrier. The ratio $\alpha = \nu'/\nu$ of the hopping rates for on-terrace jumps (3) and

$$\nu' = \nu_0 \mathrm{e}^{-E_{\mathrm{S}}/(k_{\mathrm{B}}T)} \tag{13}$$

for step edge crossings, can be used to obtain the additional step edge barrier ΔE_{ES} between the barrier for on-island diffusion E_{D} and the barrier for step crossing E_{S}. It is crucial to realize at this point that ν', and therefore also ΔE_{ES}, can only be effective values for interlayer mass transport. Different edge terminations can in fact have very different hopping rates and barriers. It is important to note that of all involved processes the one with the smallest energy barrier will be the dominant one, provided that the morphology connected with it occurs frequently [24]. A very good review on mound formation can be found in [2].

Prototypical examples of mound formation in thin films formed by rod-like molecules can be found, in particular, for pentacene [9, 129] and para-Sexiphenyl [76]. Figure 9 gives an overview on the morphology of growth mounds formed by 6P on a sputtered mica surface at 300 K. Careful sputtering of the crystalline mica (0001) surface destroys the symmetry of the surface and results in an disordered surface with an unchanged chemical composition [76, 92]. This modification reorients the otherwise flat-lying molecules into an upright orientation. With increasing film thickness pronounced mounds start to form on the mica surface. As can be seen from figure 10 and the corresponding cross section, the mounds are formed from upright standing molecules and exhibit an irregular hexagonal shape. The steep trenches and the change in curvature of the mound slope that characterizes this morphology are an experimental verification of the Zeno Paradox described by Elkinani and Villain [124].

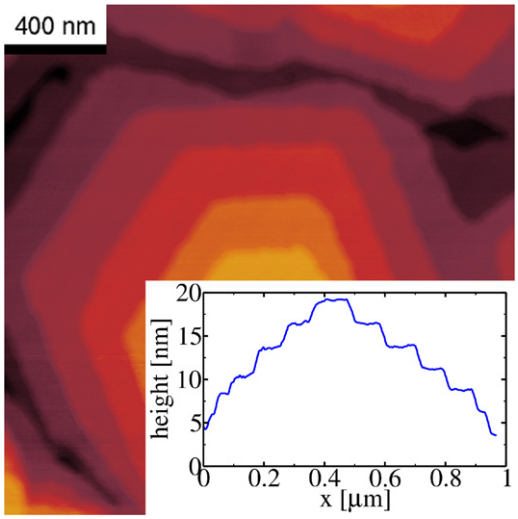

Figure 10. Individual hexagonal-shaped 6P mound and corresponding cross section. Single 2.7 nm high terraces can be identified.

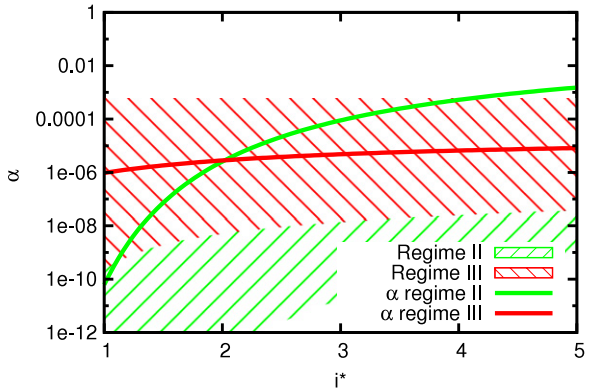

Figure 11. Probability α for step edge crossing for different i^*. Solutions for regime II (green line) are only valid for $i^* = 1$. The curve exceeds the valid range (green hatched area) for a larger critical nucleus. Solutions for regime III (red hatched area) are well within the bounds $\Gamma^{-\delta_1} \ll \alpha \ll \Gamma^{-\chi/2}$.

An analysis of this growth behavior [125, 130, 131] allows one to extract the step edge or Ehrlich–Schwoebel barrier active in such a system [76]. The step edge hopping rate in the system can be obtained from the top terrace diameter [125]

$$l \propto \left(\frac{\nu'}{F}\right)^{\frac{1}{5}}. \tag{14}$$

The size of the top terrace is limited by the fact that, for terraces larger than l, nucleation will occur on top of it, making it the second to top terrace. For the above-presented film, l has been measured to be 40 nm ± 20 nm [76]. The probability for such a nucleation event is related to the ratio between Δt (11) and the residence time τ (12). The hopping rate for the on-terrace diffusion can be obtained from kinetic nucleation theory [5], which relates the nucleation density $N = 1/\lambda^2$ to the hopping rate ν and the flux F via (2). The average island distance λ is measured to be 1 μm [76] for the film presented in figure 9. The relevant time scales here are again Δt (11) and the traversal time τ_{tr} (10). The fact that the so-obtained value for $\Delta E_{\mathrm{ES}} = 0.67$ eV is 30 times higher than the barrier for 6P diffusion on top of a 6P(001) terrace (0.02 eV determined by molecular dynamics calculations [76]) gives rise to the pronounced mound formation in this system. Such high barriers are not uncommon for organic systems. Fendrich *et al* report 0.78 eV for the Ehrlich–Schwoebel barrier of flat-lying 3,4,9,10-perylene-tetracarboxylic-dianhydride (PTCDA) on PTCDA(102) using empirical potentials and the nudged elastic band method [132]. For both systems—6P and PTCDA—the calculated diffusion barrier on the terraces is smaller by at least one order of magnitude.

However, further careful analysis shows that the above method is only valid for the case of $i^* = 1$. As we have seen in section 2.1 (figure 4), this is rarely the case in organic systems [62, 85]. Following the arguments of [126] we obtain

$$l \sim \Gamma^{\gamma'} \alpha^{\mu'} \tag{15}$$

with $\Gamma \equiv \nu/F$. Depending on the detailed balance of the above-presented time scales (10)–(12), one arrives at one of four possible regimes. For regime I, where $\alpha \ll \Gamma^{-1}$, we obtain pure Poisson growth. Regime II extends from $\Gamma^{-1} \ll \alpha \ll \Gamma^{-\delta_1}$, where $\delta_1 = i^*(2i^* - 1)/(2i^*(i^* + 1) + 2) < 1$ for all i^*. The exponents in (15) are then given by

$$\gamma' = \mu' = \frac{i^*}{3i^* + 2}. \tag{16}$$

For larger values of α, but still smaller than $\Gamma^{-\chi/2}$, the exponents take the form

$$\gamma' = \frac{i^*}{i^* + 3}, \qquad \mu' = \frac{i^* + 1}{i^* + 3}. \tag{17}$$

For $\alpha > \Gamma^{-\chi/2}$, we enter the regime of weak barriers and the mound cross section starts to deviate from the above-presented wedding cake shape. Figure 11 plots the evolution of α in regime II and III for different i^*, together with the extent of their validity. As one can immediately recognize, regime II is only valid for the case of $i^* = 1$. The value of $\alpha \approx 2 \times 10^{-10}$ can be expressed in terms of the step edge barrier using (3) and (13). The exponential prefactors ν_0 and ν_0' are assumed to be equal. As the current regime II reproduces the scenario used in [76], we obtain a similar result of $\Delta E_{\mathrm{ES}} = 0.58$ eV. The difference is attributed to the factor of probability, which has a small effect on the final result and is neglected for this overview. This result is only valid if the pair dissociation time $\tau_{\mathrm{dis}} \gg \tau_{\mathrm{tr}}^2/\tau$, which is not the case for $i^* > 1$. We do find valid solutions for $\tau_{\mathrm{dis}} \ll \tau_{\mathrm{tr}}^2/\tau$ (this regime III in [126, 133] corresponds to regime I in [125]). A smaller barrier of $\Delta E_{\mathrm{ES}} = 0.36$ eV is obtained in this regime. From figure 11 one can see that there is a weak dependency of α on i^*. However, the change is within the error bar of the experimental data used as input for the calculation. As discussed above, for values of α above or below the marked regions II and III one enters pure Poisson

growth or the weak barrier regime. Please note that for larger i^*, regime III splits into a fluctuation and a mean-field regime with identical scaling exponents, and the evolution presented in figure 11 has to be carefully reviewed for $i^* > 2$. The difference being that for a small number of involved particles the common mean-field approach is not valid. The above-presented method—taking into account the statistical nature of the initial nucleation—is needed in the case of small numbers. The complete phase diagram of $-\ln\alpha/\ln\Gamma$ versus i^* can be found in [126]. However, taking into account the size and dimensionality of the building blocks we expect the fluctuation-governed regime to be valid for larger i^* values than for atomistic processes.

However, the barrier—even for the same edge—must not necessarily be constant during thin-film growth. Two things have been revealed for the initial growth of 6P on sputtered mica (see figure 6(d)). First, for the given film thickness too few second-layer islands have nucleated. Second, the islands are only 2 nm high, indicating a larger tilt angle for the molecules. As a result, a value of $\Delta E_{\mathrm{ES}} = 0.26$ eV is reported for the first-layer ESB in [76] using the method presented in [125]. However, following the arguments presented above, this calculation and the size of the resulting step edge barrier has to be carefully revisited. The analysis based on [126] shows that only for regime III can a valid solution be found. In regime III the critical islands size for second-layer nucleation

$$L_{\mathrm{c}} \sim \Gamma^{\gamma}\alpha^{\mu} \tag{18}$$

can be calculated using the exponents

$$\gamma = \frac{\chi + i^*}{i^* + 5}, \qquad \text{and} \qquad \mu = \frac{i^* + 1}{i^* + 5}. \tag{19}$$

An additional problem in this calculation arises from the fact that in

$$f = 1 - \mathrm{e}^{-(\frac{L}{L_{\mathrm{c}}})^{k+2}} \tag{20}$$

which relates the second-layer island fraction f to the critical island size for nucleation we find the exponent k. This exponent k is known to be 5 for fluctuation-controlled nucleation in regime II in the case that $i^* = 1$ [125]. By comparing (15) with (18) in [126] and (21) and (22) in [125] we obtain the general expression for regime III $k = i^* + 3$. The result of these considerations used in (18)–(20) is plotted in figure 12. The red curve shows the expected α for different i^* in regime III. Although this curve ranges within its limits $\alpha_X = \alpha^{1/(2i^*-1)} \gg \alpha \gg \alpha^{-1/3}\lambda^{-2/(3\chi)} = \alpha_F$ for small and large i^*, the general condition for the validity of the fluctuation-controlled regime

$$\chi < \frac{2}{i^* + 1} \tag{21}$$

limits its extent to values of $i^* \leq 2$. For larger values of i^* the mean-field approach from [133] becomes valid. Based on the expressions (8b) and (7) in [133] we obtain

$$R_{\mathrm{c2}} \sim \left[(i^* + 5)\frac{L^2}{2\pi^3}4^{i^*}\left(\frac{1}{2}\right)^{i^*+1}\lambda^{2(i^*+2)}\alpha^{i^*+1}\right]^{\frac{1}{i^*+5}} \tag{22}$$

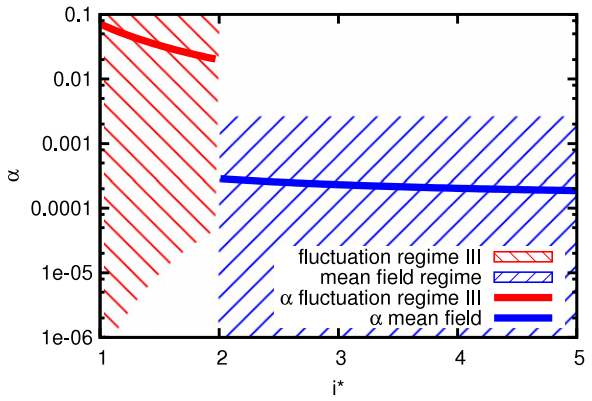

Figure 12. Probability for step edge crossing for different i^*. The solution in regime III is plotted in red together with the range of applicability. For $i^* > 2$ the fluctuation-controlled method becomes invalid and the mean-field approach (blue) becomes valid.

and

$$f = 1 - \mathrm{e}^{-(\frac{L}{L_{\mathrm{c}}})^{m}} \tag{23}$$

for the critical island radius (22) and the second-layer island fraction (23). For the limit of high barriers—so that $\alpha \ll 2/R_{\mathrm{c}}$—the exponent has the form $m = 2i^* + 6$. The result is plotted in blue in figure 12. Based on this new analysis of the second-layer nucleation we obtain a step edge barrier $\Delta E_{\mathrm{ES}} \approx 0.1$ eV in the fluctuation-controlled regime for $i^* \leq 2$. For larger i^* values, as we deal with here, we obtain $\Delta E_{\mathrm{ES}} \approx 0.2$ eV using the mean field approach. The latter result has only a very weak dependence on i^*. The value of ΔE_{ES} for second-layer nucleation of at least 0.1 eV is substantially different from the above-presented result obtained from the Zeno Paradox and the overall mound shape of thicker films ($\Delta E_{\mathrm{ES}} = 0.36$ eV). The observed change in molecular tilt angle for the first few layers [76] can explain this discrepancy. A molecule crossing the step edge with its long molecular axis roughly perpendicular will bend over the edge while descending. As the molecular tilt in the (001) plane gets smaller the necessary bending, and thus the required energy, gets smaller as well.

The situation for a nucleus formed by flat-lying molecules is more complicated, since we cannot estimate the order of the dimer dissociation time from the finite dimer energy. In addition, sterical hindering during the nucleation starts to play a role and one enters the regime of ALA [85]. In principle, the above considerations can be extended into this regime. For such a situation the exponent in (2) takes the form $\chi = 2i^*/(i^* + 3)$ [134]. In addition, the growth laws—forming the foundation for the calculation—will play an important role.

When the molecule crosses the step edge it performs a complicated sequence of twisting, rotating, and bending [77]. All these processes are costly in terms of energy, and add to the final barrier height the molecule has to overcome. However, the molecule will take the pathway for which all contributions are added in such a way that the final barrier will be minimal. In particular, for a molecule crossing the step edge with the long axis roughly perpendicular to the edge,

the bending energy is a significant contribution. A decreased tilt of the molecular backbone during the crossing lowers this energy term and, consequently, the overall barrier height.

The existing studies demonstrate that the prediction of barrier heights is complicated and full of pitfalls. For the presented case, a good agreement has been achieved initially between theory and experiment. The analysis assumed a molecule that crosses the step edge with the long axis perpendicular to the edge [76]. However, after relaxing some of the constraints used, other trajectories—with lower barriers (($\Delta E_{ES} = 0.34$ eV))—involving difficult *Fosbury Flop*-like movements at the step edge were found [77]. The above-presented new analysis of the experimental data is in good agreement with the evolved molecular dynamics simulations that predict a complicated step edge crossing process and comparable barriers. Focused research in this direction is important, as mound formation and layer-dependent ESB values are common in organic thin-film growth. A level-dependent ESB (e.g. as described above and in [76, 135]) often goes hand in hand with a change in tilt angle of the molecular backbone. However, the proposed *Fosbury Flop*-like step edge crossing cannot explain the experimentally observed step edge barrier reduction. Provided the ESB becomes small enough then the initial layers can completely close [135]. Other examples include the growth of DIP on native SiO_x, which is characterized by a transition from LbL growth to mound growth. This is explained by changes in the interlayer mass transport [119].

Care has to be taken when comparing experimental results with simulations and DFT-based calculations. It is important to realize that the experimentally obtained barriers based on averaged mound shapes represent the effective barrier in the entire film. Using well-defined step edges (the (100) in [76, 77]) allows a detailed insight into the dynamics of the step edge crossing for the specific facet. However, the elongated hexagonal shape of the 6P islands (see figure 10) has at maximum two of these (100) step edges. In addition, these two (the (100) and the ($\bar{1}$00)) will also have different tilt directions (inward and outward tilt) with respect to the top surface, which in turn are both different from the tilt angle of the other unit cell facets (the vertical (010) facet) and other possible step edges. This and other peculiarities of molecular step edges (see also appendix B in [77]) show how difficult it is to make precise predictions of experimentally obtained values for step edge barriers.

3.2. Growth of three-dimensional islands and fibers

Although smooth films are usually preferred, the crystalline and one-dimensional nanofibers presented in figures 6(a) and (b) are one out of many examples of a useful non-smooth morphology. It is important to remember that these anisotropic structures grow from flat-lying molecules. The section 3.1 dealt with upright standing molecules where no or only a weak anisotropy in the substrate plane can be expected. In particular, the fact that blue lasing [115, 136] has been shown for these fibers and that they can be used as waveguides [137] opens several possibilities for applications.

Two cases have to be separated here. While often three-dimensional fibers grow directly on the substrate (Volmer–Weber growth), in particular the fibers found on mica grow on a metastable wetting layer (Stranski–Krastanov growth). In both cases the molecule–molecule interaction dominates over the molecule–substrate interaction. The difference between these two types of interaction is large enough to facilitate the rearrangement and reorientation of entire crystallites as entities.

The rearrangement of crystallites containing more than 140 000 molecules is observed during the HWE deposition of 6P onto crystalline mica (0001) at 360 K [88]. During the deposition of 6P, first a wetting layer is formed. With increasing coverage, crystallites grow on this wetting layer. However, after a critical amount of 6P has been deposited a rearrangement takes place and fibers—formed by the already existing crystallites—become the dominant morphological feature. Figure 6(a) shows such a chain of crystallites. The particular arrangement of the individual chains with respect to each other (see figure 13(a)) is explained by a strain relaxation mechanism at work in this system [88]. The stress induced by the crystallites in the wetting layer leads to the formation of a defect network (indicated by green lines in figure 13(a)) that guides the rearrangement process of the crystallites. It is important to realize at this point that during this rearrangement process the crystallites move as entities. This relocation of whole 6P crystallites on mica (0001) is possible due to the delicate balance between the strong intermolecular interaction and the rather weak film substrate interaction. Detailed x-ray diffraction (XRD) studies have revealed the epitaxial relationship between 6P and the mica (0001) surface [14, 138]. In particular, they have shown that once the formation of needles sets in, the initially compressed spacing of the (11$\bar{1}$) planes quickly relaxes towards the bulk value [139].

Recently, a bimodal size distribution for the crystallites on crystalline mica has been observed. However, this behavior for ultra-thin layers at a slightly elevated temperature of 400 K is only observed after exposing the samples to ambient conditions. Using TDS before and after exposing the sample to ambient conditions as well as AFM revealed that the initial present wetting layer is transformed into small crystallites. This second generation of smaller crystallites forms between the already existing fibers or chains of crystallites [140]. For thicker films, the material from the wetting layer is most likely captured by the large number of existing big crystallites and fibers. In figure 13(b), a thick film where long 6P needles have formed is presented. Several small second generation crystals are visible in the inset of figure 13(b).

As we have seen for the case of crystalline mica versus sputtered mica, the substrate plays an important role in the determination of the molecular orientation. However, also a particular surface reconstruction can provide an interesting growth template. The (1×1) reconstruction of the $TiO_2\{110\}$ surface is characterized by parallel rows of protruding oxygen atoms. These rows run along the [001] azimuth [141]. The spacing of 6.5 Å is sufficient to accommodate the width of a 6P molecule. Deposition of 1.3 ML of 6P at 400 K leads to

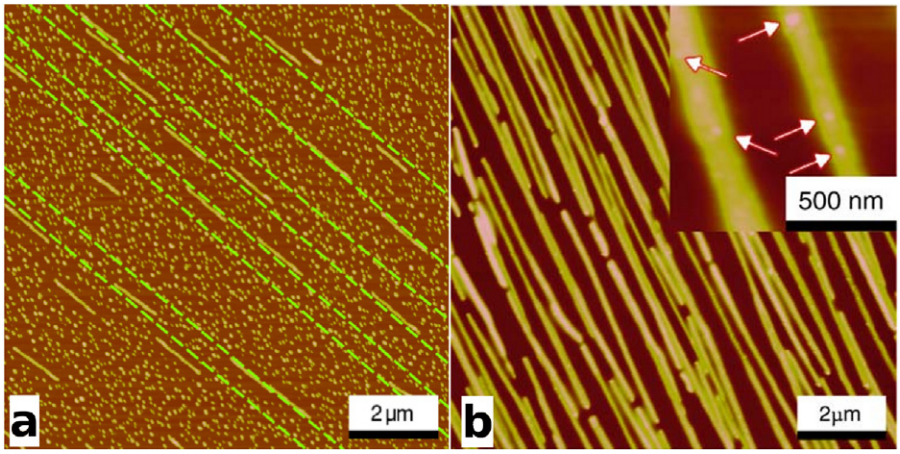

Figure 13. AFM images of HWE-grown 6P fibers on mica (0001). (a) Fibers—formed by a rearrangement process of several individual crystallites—line up on a dislocation network (indicated by green dashed lines) present in the wetting layer. (b) Detail of 6P crystallite chains with a length of several μm, grown on clean mica under HV conditions. The high-resolution inset reveals the presence of small crystallites decorating the fibers. Reprinted from [88]. With kind permission from Springer Science and Business Media.

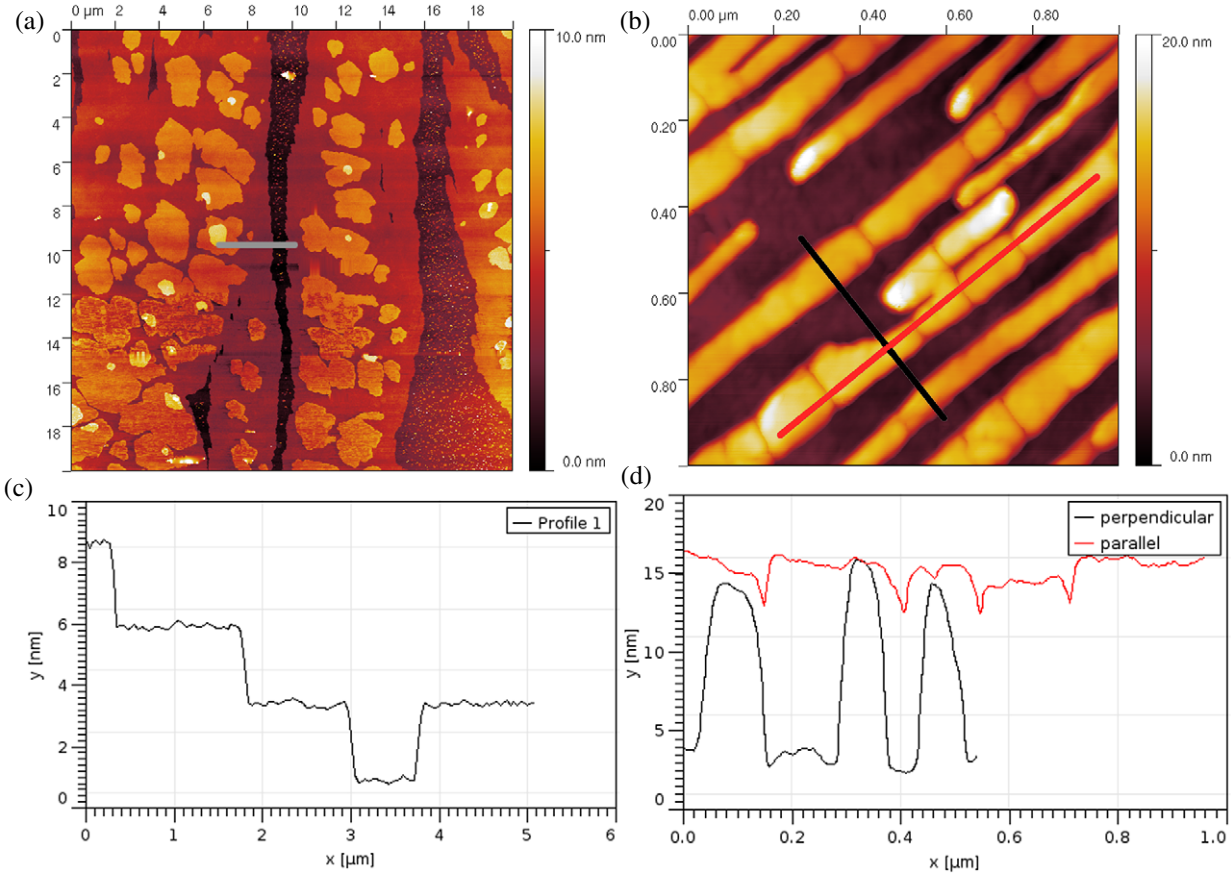

Figure 14. 6P deposition on $TiO_2\{110\}$-(1×1) [143]. (a) High-temperature deposition at 400 K leads to the formation of elongated islands formed by upright standing molecules. (b) Low-temperature deposition at 300 K results in the formation of long 6P fibers. Please note that the orientation of the structures has rotated by 90° from [001] to [1$\bar{1}$0]. (c), (d) Cross-sections along the lines indicated in (a) and (b).

the formation of large islands formed from upright standing molecules presented in figure 14(a). The islands are separated by trenches filled with small crystallites which are a few monolayers high. The trenches run parallel to the oxygen rows along the [001] azimuth of the $TiO_2\{110\}$ surface [142]. The islands themselves are polycrystalline, with four domains symmetrically spaced around the [001] direction. With a size of only 300 nm $\times$ 30 nm, these domains are much smaller than the several μm large islands they form. The long axis of these domains is also oriented along the [001] direction [144].

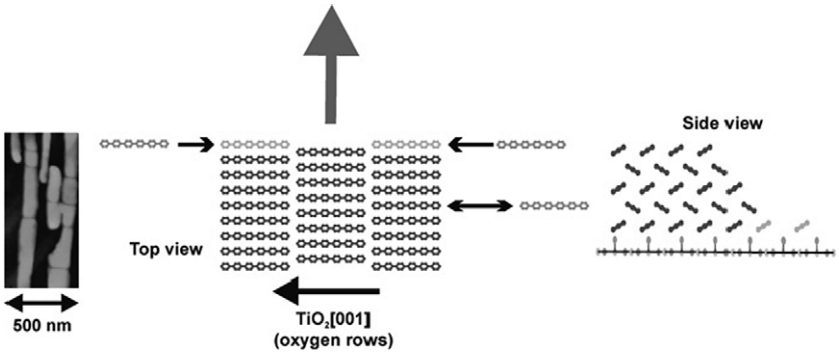

Figure 15. Sticking anisotropy for 6P on TiO_2. The fibers shown in the AFM image (z-scale: 30 nm) on the left grow along the $[1\bar{1}0]$. The sketch shows the molecular arrangement from the top and the side. The gray arrow indicates the growth direction. Reprinted from [145]. Copyright (2006), with permission from Elsevier.

The reason for this growth behavior is rooted in the diffusion anisotropy present on this surface. The molecules can easily diffuse along the [001] direction guided by the oxygen rows. Analyzing the width of the area in the trenches which is depleted from the small crystallites, one arrives at a ratio for the anisotropy between the diffusion along [001] and $[1\bar{1}0]$ of 4–64 [145]. This is clearly a property of the $TiO_2\{110\}$-(1×1) substrate surface, since second- and third-layer islands show an isotropic shape. All these structures formed by upright standing molecules grow on top of a wetting layer of flat-lying molecules [146]. Such flat-lying to upright transitions have been observed for 5A on Cu{110} [147] and other systems. For 5A on Cu{110}, the transition involves a flat-lying wetting layer, which is followed by an intermediate layer having a herringbone structure with the long molecular axis parallel to the substrate. For layers thicker than 2 nm an upright standing orientation is found in this system.

Lowering the growth temperature to 300 K results in a complete change of growth morphology, molecular orientation, and mesoscopic structure orientation. The morphology presented in figure 14(b) is characterized by long and high polycrystalline 6P fibers. It is important to realize that these fibers run parallel to the $[1\bar{1}0]$ and thus perpendicular to the oxygen rows and the trenches observed at higher temperatures. These fibers are formed from flat-lying molecules that have their long axis roughly parallel to the substrate surface and are oriented along the [001] direction of the $TiO_2\{110\}$ surface. In addition to the diffusion anisotropy active at high temperatures, here the sticking probability for molecules to be incorporated into existing fibers plays an important role. The long side walls of the fibers are terminated by the hydrogen atoms at the long end of the molecules. This has to be compared to the short side of the fiber, where the π systems of the molecules are exposed. It is clear that the sticking probability at the short end will be substantially higher. Consequently, the fibers will grow quickly along $[1\bar{1}0]$, but slower in width. An illustration of the situation is shown in figure 15.

An interesting mesoscopic approach to orient the fiber growth has been shown by Madsen *et al* [148]. They used arrays of gold-coated micro-ridges. By tuning the ridge width and deposition temperature, 6P fibers growing perpendicular to the ridges could be grown with a high yield.

3.3. Layer-by-layer growth of flat-lying molecules

Although the above-mentioned needle-like morphology might be useful for special applications, a smooth interface is required for most applications. This is in particular related to the fact that a lower number of defects at the interface facilitates higher charge carrier mobilities [19–22]. As we have seen above, films formed by upright standing molecules suffer in many cases from high step edge barriers that will ultimately lead to mound formation and rough interfaces. So far, efforts to obtain layer-by-layer growth have led only to limited success.

Wu *et al* have achieved five layers in the desired LbL growth for the important case of 5A on SiO_x by using SuMBD [149]. Using conventional OMBD, Zhang *et al* showed the strain-relaxation-driven transition from LbL to rapid roughening after 5 layers for the plate-like molecule DIP [150]. In both studies, films formed from upright standing molecules have formed. However, some success has been obtained for flat-lying molecules.

Recently, layer-by-layer growth of flat-lying molecules has been obtained for 6P on the technologically important substrate graphene [151–153]. Graphene [154, 155] can be used as a transparent, flexible and highly conductive electrode for organic electronic applications [156, 157]. The combination of optically active films of flat-lying molecules on transparent electrode materials is a promising route to high-efficiency OLEDs.

The formation of the 6P film in LbL mode at 240 K has been monitored using *in situ* real-time low-energy electron microscopy (LEEM) and micro low-energy electron diffraction (μLEED) for structural characterization. The growth proceeds via a multi-step process that involves the reorientation of a significant portion of already deposited molecules [151]. The process starts with the formation of a metastable layer of exclusively flat-lying molecules (depicted in figure 16(A)). With ongoing deposition, this highly mobile initial layer [78, 153] transforms into a stable immobile layer having a higher packing density and a bulk-like arrangement of the molecules (see figure 16(B)). The structure of this stable layer corresponds to the $(1\bar{1}1)$ plane of 6P. A similar growth process for the first monolayer has been reported

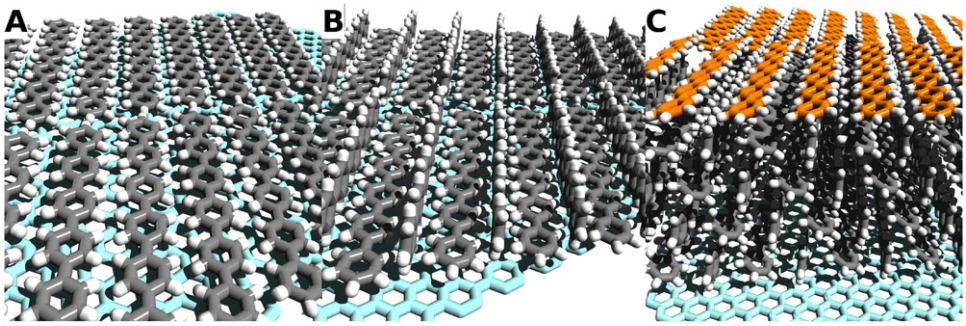

Figure 16. Structural model of a 6P thin film grown on metal-supported graphene (light blue hexagonal layer) at 240 K. (A) The initial metastable layer is formed from flat-lying molecules (gray carbon atoms) only. (B) After reaching a critical coverage, the structure changes to a bulk-like molecular arrangement. This is achieved by tilting parts of the molecules on the long edge, as well as directly inserting molecules from the gas phase. (C) The film grows in LbL mode by a repetition of the previous two steps. The bulk of the thin film has a Baker-like structure [15] and exposes the $(1\overline{1}\overline{1})$ plane to the underlying graphene substrate. The topmost layer (orange carbon atoms) is not completed and shows a metastable structure consisting of flat-lying molecules only. Adapted with permission from [151]. Copyright (2011) American Chemical Society.

for 6P on Au{111} [69]. However, on gold the growth at or above room temperature results in three-dimensional growth. It is important to understand the significance of the substrate for this process. Although earlier STM studies of 6P on graphite [158] also report flat-lying molecules, the epitaxial relationship there is different frpm the one found on metal-supported graphene. Using empirical force fields and total energy calculations it could be shown that indeed a different alignment of the long molecular axis is favored on the two substrates [151]. The layer-by-layer growth process continues with the repetition of the above two steps [151]. Every additional layer starts with the formation of the metastable initial layer of only flat-lying molecules that transforms into a layer with the bulk structure once a critical coverage is reached. Figure 16(C) shows the final film structure obtained by (μLEED) for 4.5 ML coverage. The achieved thin-film structure shows the potential for high-efficiency OLED structures on a transparent and flexible substrate [151].

4. Conclusion

In the first part of this review we discussed the nucleation and growth behavior of rod-like molecules. We presented several methods to determine the critical nucleus size. However, we also showed that due to the non-zero-dimensional nature of the molecules, care has to be taken when using formalisms originally introduced for atomic diffusion processes. Many problems—originally identified in inorganic systems—return in organic thin-film growth. While phenomena such as attachment-limited aggregation have been observed in a few inorganic systems, they are encountered on a regular basis in organic systems. However, the biggest difference is due to the reorientation processes involved in the growth of films formed by upright standing molecules. Initial insight is gained mostly by using computational methods, as the actual processes are difficult to monitor experimentally. The most difficult question to answer is related to the definition of the critical nucleus. Is an immobile cluster of flat-lying molecules that finally nucleates a film formed by upright standing molecules the critical nucleus in a strict homoepitaxial sense? Although this is to a certain level a semantic question, one has to realize that most experimental techniques to determine i^* are insensitive to the orientation of the molecules. Consequently, this problem needs to be discussed when interpreting the results.

Furthermore, the molecular orientation plays a crucial role in defining the efficiency of organic electronic devices. We have shown several ways to influence the orientation. We pointed out that substrate order and defects plays a crucial role for switching from films formed by flat-lying molecules to films made from upright standing molecules.

In the second part of this review we focused on diffusion processes that define the final film morphology. We extensively discussed mound formation in the presence of an effective Ehrlich–Schwoebel barrier and, in particular, the theoretical problems that arise when the critical nucleus becomes large. However, as expected, a larger i^* will not lead to a decrease of the involved step edge barriers. Two additional remarks have to be added to this discussion. First, given the size and the additional rotational degrees of freedom of molecules compared to atoms, the transition from the fluctuation-determined regime to the mean-field regime probably occurs at larger i^* than in inorganic growth. Second, we briefly discussed how to extract the critical nucleus sizes for attachment-limited aggregation (ALA) and diffusion-limited aggregation (DLA). The latter is also observed in organic growth and leads to the formation of ramified islands. In the case of ALA, fewer molecules arrive at the lower step edge, thus reducing the upward diffusion flux. For reasonable barrier heights this should facilitate LbL-like growth. In the case of DLA, the number of kink sites increases substantially, creating more low-barrier pathways over the step edge. While, for ALA, edge diffusion is in principle possible, this mechanism is not effective in DLA. Consequently, more and longer undesired domain boundaries are expected for DLA growth. The process of mound formation and its relation to layer-by-layer growth gets

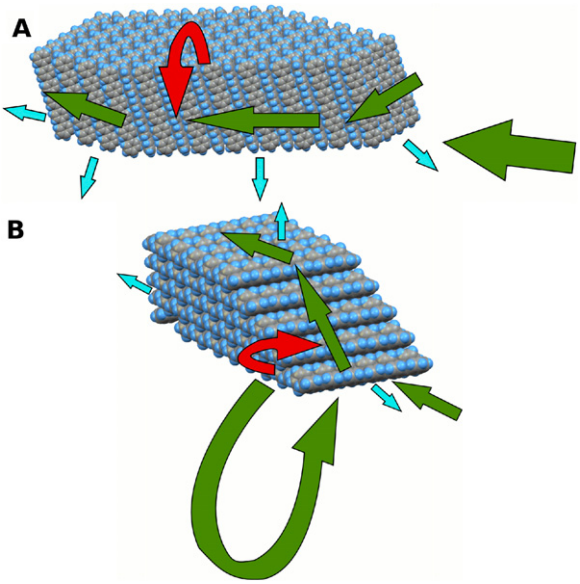

Figure 17. Sketch highlighting probable (green) and less probable (red) diffusion paths for rod-like organic molecules. The same diffusion paths with nearly identical barriers (ignoring the substrate effect) exist for structures formed from either upright or flat-lying molecules. While for upright standing molecules the red process is forbidden due to a high ESB, this process can be circumvented for structures formed by flat-lying molecules.

further complicated by the fact that the ESB can be layer dependent. Often in organic epitaxy a change of molecular tilt angle is the root cause for this change of the barrier height and the growth mode.

Self-organization of the formed nano-structures can effectively be controlled by balancing the anisotropies present within the growth system. This includes—but is not limited to—diffusion and sticking anisotropy as well as the anisotropy of the substrate on an atomic, but also mesoscopic length scale. Also wetting layers play an important role for many organic systems. They are not necessarily stable under ambient conditions. However, rearrangement processes mediated by the wetting layer—like the one observed for the crystallite chain formation—can therefore only happen during (U)HV growth. No change of morphology by such a process is possible once the wetting layer has dissolved.

In general, the anisotropy of the molecules leads to an anisotropy between the different diffusion processes. However, depending on the actual orientation of the molecules with respect to the substrate the diffusion pathways change their meaning. The path indicated by the red arrow in figure 17(A) for the step edge crossing has a low probability and results in the undesired mound formation. However, for the case of flat-lying molecules (figure 17(B)), the same diffusion process can actively be avoided. The small sticking probability at—what is now—the side of the fiber, allows the molecules to circumvent the red diffusion process by returning into the gas phase and reattachment at the small end. The consequence is the often observed fiber growth perpendicular to the long molecular axis. The same analogy holds for edge diffusion (upright standing molecules) and up-hill diffusion (flat-lying molecules).

Finally, we presented results of LbL growth of rod-like molecules and illustrated the often complicated rearrangement process occurring during growth of organic thin films (such as for the above-described low-temperature growth of 6P on graphene). Similar to above, a deviation from the bulk structure goes hand in hand with a change of growth mode—in this case from three-dimensional needles to layer-by-layer growth of flat-lying molecules. The involved metastable islands exhibit an interesting diffusion behavior which is mediated by a delicate interplay of strains in film and substrate.

Considering the above-presented information, two issues become immediately evident. Forcing the molecules to deviate from their desired bulk structure results in new and interesting growth phenomena and presents a viable route for controlling the film morphology. Secondly, the level of understanding of organic thin-film epitaxy has increased dramatically within the past decade. However, there is still a large number of open questions. Having identified these questions, dedicated experiments—supported by computational methods—have to be designed to answer the existing challenges.

Acknowledgments

We grateful acknowledge all the people who were involved in the original research funded by the Austrian Science Fund (FWF) under Projects No P19197, S9707, and S9714. In particular Claudia Ambrosch-Draxl, Andree Andreev, Stephen Berkebile, Paul Frank, Stefan Lorbek, Stefan Müllegger, Bene Poelsema, Peter Puschnig, Mike Ramsey, Roland Resel, Serdar Sariciftci, Quan Shen, Helmut Sitter, Raoul van Gastel, and Adi Winkler. In addition we want to express our thanks to Andrei Kadashchuk and Horst-Günter Rubahn. Finally we want to thank Harold J W Zandvliet for making this manuscript possible.

References

[1] Markov I V 2003 *Crystal Growth for Beginners: Fundamentals of Nucleation, Crystal Growth, and Epitaxy* 2nd edn, (Singapore: World Scientific)
[2] Michely T and Krug J 2004 *Islands, Mounds and Atoms* (*Springer Series in Surface Sciences* vol 42) (Berlin: Springer)
[3] Brune H 1998 *Surf. Sci. Rep.* **31** 125–229
[4] Ratsch C and Venables J A 2003 *J. Vac. Sci. Technol.* A **21** S96–109
[5] Venables J A, Spiller G D T and Hanbucken M 1984 *Rep. Prog. Phys.* **47** 399–459
[6] Wagner S and Bauer S 2012 *MRS Bull.* **37** 207–13
[7] Campione M, Caprioli S, Moret M and Sassella A 2007 *J. Phys. Chem.* C **111** 12741–6
[8] Ruiz R, Nickel B, Koch N, Feldman L, Haglund R, Kahn A, Family F and Scoles G 2003 *Phys. Rev. Lett.* **91** 136102
[9] Stadlober B, Haas U, Maresch H and Haase A 2006 *Phys. Rev.* B **74** 165302
[10] Yang J, Wang T, Wang H, Zhu F, Li G and Yan D 2008 *J. Phys. Chem.* B **112** 7816–20
[11] Ruiz R, Choudhary D, Nickel B, Toccoli T, Chang K C, Mayer A C, Clancy P, Blakely J M, Headrick R L,

Iannotta S and Malliaras G G 2004 *Chem. Mater.* **16** 4497–508
[12] Fichou D (ed) 1999 *Handbook of Oligo- and Polythiophenes* (Weinheim: Wiley–VCH)
[13] Horowitz G, Fichou D, Peng X and Garnier F 1991 *Synth. Met.* **41** 1127–30
[14] Resel R 2003 *Thin Solid Films* **433** 1–11
[15] Baker K N, Fratini A V, Resch T, Knachel H C, Adams W W, Socci E P and Farmer B L 1993 *Polymer* **34** 1571–87
[16] de Boer R W I, Gershenson M E, Morpurgo A F and Podzorov V 2004 *Phys. Status Solidi* a **201** 1302–31
[17] Hu W S, Tao Y T, Chen Y F and Chang C S 2008 *Appl. Phys. Lett.* **93** 053304
[18] Bauer E 1958 *Z. Kristallogr.* **110** 372–94
[19] Fritz S E, Kelley T W and Frisbie C D 2005 *J. Phys. Chem.* B **109** 10574–7
[20] Steudel S, De Vusser S, De Jonge S, Janssen D, Verlaak S, Genoe J and Heremans P 2004 *Appl. Phys. Lett.* **85** 4400–2
[21] Yan H, Swaraj S, Wang C, Hwang I, Greenham N C, Groves C, Ade H and McNeill C R 2010 *Adv. Funct. Mater.* **20** 4329–37
[22] Schumacher D and Stark D 1982 *Surf. Sci.* **123** 384–96
[23] Teichert C 2002 *Phys. Rep.* **365** 335–432
[24] Teichert C, Ammer C and Klaua M 1994 *Phys. Status Solidi* A **146** 223–42
[25] Ehrlich G and Hudda F G 1966 *J. Chem. Phys.* **44** 1039–49
[26] Schwoebel R L and Shipsey E J 1966 *J. Appl. Phys.* **37** 3682–6
[27] Dodabalapur A, Torsi L and Katz H E 1995 *Science* **268** 270–1
[28] Volmer M 1913 *Ann. Phys.* **345** 775–96
[29] Koenigsberger J and Schilling K 1910 *Ann. Phys.* **337** 179–230
[30] Pope M, Kallmann H P and Magnante P 1963 *J. Chem. Phys.* **38** 2042–3
[31] Helfrich W and Schneider W 1965 *Phys. Rev. Lett.* **14** 229–31
[32] Chiang C, Fincher C, Park Y, Heeger A, Shirakawa H, Louis E, Gau S and MacDiarmid A 1977 *Phys. Rev. Lett.* **39** 1098–101
[33] Tang C W 1986 *Appl. Phys. Lett.* **48** 183–5
[34] Horowitz G, Fichou D, Peng X, Xu Z and Garnier F 1989 *Solid State Commun.* **72** 381–4
[35] Koezuka H, Tsumura A and Ando T 1987 *Synth. Met.* **18** 699–704
[36] Burroughes J H, Jones C A and Friend R H 1988 *Nature* **335** 137–41
[37] Burroughes J H, Bradley D D C, Brown A R, Marks R N, Mackay K, Friend R H, Burns P L and Holmes A B 1990 *Nature* **347** 539–41
[38] Braun D and Heeger A J 1991 *Appl. Phys. Lett.* **58** 1982–4
[39] Tang C W and Van Slyke S A 1987 *Appl. Phys. Lett.* **51** 913–5
[40] Tang C W, Van Slyke S A and Chen C H 1989 *J. Appl. Phys.* **65** 3610–6
[41] Reese C, Roberts M, Ling M and Bao Z 2004 *Mater. Today* **7** 20–7
[42] Samuel I D and Turnbull G A 2004 *Mater. Today* **7** 28–35
[43] Sariciftci N S 2004 *Mater. Today* **7** 36–40
[44] Borchardt J K 2004 *Mater. Today* **7** 42–6
[45] Brütting W (ed) 2005 *Physics of Organic Semiconductors* 1st edn (Weinheim: Wiley-VCH)
[46] Swartzentruber B S 1996 *Phys. Rev. Lett.* **76** 459–62
[47] Paserba K R and Gellman A J 2001 *Phys. Rev. Lett.* **86** 4338–41
[48] Fichthorn K A and Miron R 2002 *Phys. Rev. Lett.* **89** 196103
[49] Wöll C (ed) 2009 *Physical and Chemical Aspects of Organic Electronics* (Weinheim: Wiley-VCH)
[50] Klauk H (ed) 2006 *Organic Electronics: Materials, Manufacturing, and Applications* (Weinheim: Wiley-VCH)
[51] Kiel M, Duncker K, Hagendorf C and Widdra W 2007 *Phys. Rev.* B **75** 195439
[52] Yanagi H, Okamoto S and Mikami T 1997 *Synth. Met.* **91** 91–3
[53] Yanagi H and Okamoto S 1997 *Appl. Phys. Lett.* **71** 2563–5
[54] Al-Shamery K H, Rubahn H G and Sitter H (ed) 2008 *Organic Nanostructures for Next Generation Devices* (*Springer Series in Materials Science* vol 101) (Berlin: Springer)
[55] Guha S, Graupner W, Resel R, Chandrasekhar M, Chandrasekhar H R, Glaser R and Leising G 1999 *Phys. Rev. Lett.* **82** 3625–8
[56] Bartelt M and Evans J 1992 *Phys. Rev.* B **46** 12675–87
[57] Bartelt M and Evans J 1996 *Phys. Rev.* B **54** R17359–62
[58] Amar J and Family F 1995 *Phys. Rev. Lett.* **74** 2066–9
[59] Pimpinelli A and Einstein T L 2007 *Phys. Rev. Lett.* **99** 226102
[60] Pimpinelli A and Einstein T L 2010 *Phys. Rev. Lett.* **104** 149602
[61] Mulheran P A and Blackman J A 1996 *Phys. Rev.* B **53** 10261–7
[62] Potocar T, Lorbek S, Nabok D, Shen Q, Tumbek L, Hlawacek G, Puschnig P, Ambrosch-Draxl C, Teichert C and Winkler A 2011 *Phys. Rev.* B **83** 075423
[63] Tejima M, Kita K, Kyuno K and Toriumi A 2004 *Appl. Phys. Lett.* **85** 3746–8
[64] Lorbek S, Hlawacek G and Teichert C 2011 *Eur. Phys. J.-Appl. Phys.* **55** 23902
[65] Conrad B, Gomar-Nadal E, Cullen W, Pimpinelli A, Einstein T L and Williams E 2008 *Phys. Rev.* B **77** 205328
[66] Miyamoto S, Moutanabbir O, Haller E and Itoh K 2009 *Phys. Rev.* B **79** 1–6
[67] Meyer zu Heringdorf F J, Reuter M C and Tromp R M 2004 *Appl. Phys.* A **78** 787–91
[68] Meyer zu Heringdorf F J, Reuter M C and Tromp R M 2001 *Nature* **412** 517–20
[69] Müllegger S and Winkler A 2006 *Surf. Sci.* **600** 1290–9
[70] Becker K E and Fichthorn K A 2006 *J. Chem. Phys.* **125** 184706
[71] Fichthorn K A, Becker K E and Miron R A 2007 *Catal. Today* **123** 71–6
[72] Frank P, Djuric T, Koini M, Salzmann I, Rieger R, Müllen K, Resel R, Koch N and Winkler A 2010 *J. Phys. Chem.* C **114** 6650–7
[73] Tait S L, Dohnálek Z, Campbell C T and Kay B D 2005 *J. Chem. Phys.* **122** 164708
[74] Winkler A 2009 *Thermal Desorption Of Organic Molecules Interface Controlled Organic Thin Films* (*Springer Proceedings in Physics* vol 129) ed H G Rubahn, H Sitter, G Horowitz and K Al-Shamery (Berlin: Springer) book chapter/Section 5, pp 29–36
[75] Zhdanov V 1991 *Surf. Sci. Rep.* **12** 185–242
[76] Hlawacek G, Puschnig P, Frank P, Winkler A, Ambrosch-Draxl C and Teichert C 2008 *Science* **321** 108–11
[77] Goose J E, First E L and Clancy P 2010 *Phys. Rev.* B **81** 205310
[78] Hlawacek G, Khokar F S, van Gastel R, Teichert C and Poelsema B 2011 *IBM J. Res. Dev.* **55** 15:1–7
[79] Schroeder M and Wolf D 1995 *Phys. Rev. Lett.* **74** 2062–5
[80] Filimonov S, Cherepanov V, Hervieu Y and Voigtländer B 2007 *Phys. Rev.* B **76** 035428
[81] Filimonov S N and Hervieu Y Y 2012 *Phys. Rev.* B **85** 045423
[82] Tsetseris L and Pantelides S T 2005 *Appl. Phys. Lett.* **87** 233109

[83] Andreev A, Montaigne A, Hlawacek G, Sitter H and Teichert C 2006 *J. Vac. Sci. Technol.* A **24** 1660
[84] Fichou D and Ziegler C 2007 Structure and properties of oligothiophenes in the solid state: single crystals and thin films *Handbook of Oligo- and Polythiophenes* ed D Fichou (Weinheim: Wiley-VCH) Book Chapter/Section 4, pp 183–282
[85] Tumbek L and Winkler A 2012 *Surf. Sci.* **606** L55–8
[86] Akai-Kasaya M, Ohmori C, Kawanishi T, Nashiki M, Saito A, Aono M and Kuwahara Y 2010 *Nanotechnology* **21** 365601
[87] Andreev A, Matt G, Brabec C J, Sitter H, Badt D, Seyringer H and Sariciftci N S 2000 *Adv. Mater.* **12** 629–33
[88] Teichert C, Hlawacek G, Andreev A, Sitter H, Frank P, Winkler A and Sariciftci N 2005 *Appl. Phys.* A **82** 665–9
[89] Kankate L, Balzer F, Niehus H and Rubahn H G 2009 *Thin Solid Films* **518** 130–7
[90] Balzer F, Kankate L, Niehus H and Rubahn H G 2005 Nanoaggregates from oligothiophenes and oligophenylenes: a systematic growth survey *Proc. SPIE* **5724** 285–94
[91] Rubahn H G, Sitter H, Horowitz G and Al-Shamery K (ed) 2009 *Interface Controlled Organic Thin Films* (*Springer Proceedings in Physics* vol 129) (Berlin: Springer)
[92] Frank P, Hlawacek G, Lengyel O, Satka A, Teichert C, Resel R and Winkler A 2007 *Surf. Sci.* **601** 2152–60
[93] Hlawacek G, Shen Q, Teichert C, Resel R and Smilgies D M 2007 *Surf. Sci.* **601** 2584–7
[94] Balzer F, Kintzel E J Jr, Skofronick J G, Safron S A and Rubahn H G 2003 Analysis of nanostructured blue light-emitting p-6P films on mica *Organic Light-Emitting Materials and Devices VI* vol 4800, ed I C Khoo, Seattle, WA pp 216–22
[95] Kadashchuk A, Andreev A, Sitter H, Sariciftci N S, Skryshevski Y, Piryatinski Y, Blonsky I and Meissner D 2004 *Adv. Funct. Mater.* **14** 970–8
[96] Hlawacek G, Teichert C, Müllegger S, Resel R and Winkler A 2004 *Synth. Met.* **146** 383–6
[97] Resel R, Oehzelt M, Haber T, Hlawacek G, Teichert C, Müllegger S and Winkler A 2005 *J. Cryst. Growth* **283** 397–403
[98] Müllegger S and Winkler A 2005 *Surf. Sci.* **574** 322–30
[99] Putsche B, Tumbek L and Winkler A 2012 *J. Chem. Phys.* **137** 134701
[100] Cranney M, Chalopin Y, Mayne A J and Dujardin G 2009 *Appl. Phys.* A **94** 767–73
[101] Khokhar F S, Hlawacek G, van Gastel R, Zandvliet H J W, Teichert C and Poelsema B 2012 *Surf. Sci.* **606** 475–80
[102] Conrad B, Cullen W, Riddick B and Williams E 2009 *Surf. Sci.* **603** L27–30
[103] Loi M A, da Como E, Dinelli F, Murgia M, Zamboni R, Biscarini F and Muccini M 2004 *Nature Mater.* **4** 81–5
[104] Balzer F, Beermann J, Bozhevolnyi S I, Simonsen A C and Rubahn H G 2003 *Nano Lett.* **3** 1311–4
[105] Nishimura S, Scales P J, Tateyama H, Tsunematsu K and Healy T W 1995 *Langmuir* **11** 291–5
[106] Nishimura S, Biggs S, Scales P J, Healy T W, Tsunematsu K and Tateyama T 1994 *Langmuir* **10** 4554–9
[107] Kowarik S, Gerlach A, Sellner S, Schreiber F, Pflaum J, Cavalcanti L and Konovalov O 2006 *Phys. Chem. Chem. Phys.* **8** 1834–6
[108] Dürr A C, Schreiber F, Ritley K A, Kruppa V, Krug J, Dosch H and Struth B 2003 *Phys. Rev. Lett.* **90** 016104
[109] Mikami T and Yanagi H 1998 *Appl. Phys. Lett.* **73** 563
[110] Verlaak S, Rolin C and Heremans P 2007 *J. Phys. Chem.* B **111** 139–50
[111] Verlaak S, Steudel S, Heremans P, Janssen D and Deleuze M S 2003 *Phys. Rev.* B **68** 195409
[112] Horowitz G, Hajlaoui R, Bourguiga R and Hajlaoui M 1999 *Synth. Met.* **101** 401–4
[113] Tkaczyk S W, Kityk I V and Viennois R 2004 *J. Chem. Phys.* **121** 517–24
[114] Balzer F, Bordo V G, Simonsen A C and Rubahn H G 2003 *Phys. Rev.* B **67** 115408
[115] Andreev A, Quochi F, Cordella F, Mura A, Bongiovanni G, Sitter H, Hlawacek G, Teichert C and Sariciftci N S 2006 *J. Appl. Phys.* **99** 034305
[116] Cordella F, Quochi F, Saba M, Andreev A, Sitter H, Sariciftci N S, Mura A and Bongiovanni G 2007 *Adv. Mater.* **19** 2252–6
[117] Hill I G, Weinert C M, Kreplak L and Zyl B P 2008 *Appl. Phys.* A **95** 81–7
[118] Wu Y, Toccoli T, Koch N, Iacob E, Pallaoro A, Rudolf P and Iannotta S 2007 *Phys. Rev. Lett.* **98** 076601
[119] Zhang X, Barrena E, Goswami D, de Oteyza D G, Weis C and Dosch H 2009 *Phys. Rev. Lett.* **103** 136101
[120] Zhu Y, Sun Z, Yan Z, Jin Z and Tour J M 2011 *ACS Nano* **5** 6472–9
[121] Seah M P 1972 *Surf. Sci.* **32** 703–28
[122] Meinel K, Klaua M and Bethge H 1988 *J. Cryst. Growth* **89** 447–58
[123] Elkinani I and Villain J 1994 *J. Physique I* **4** 947–73
[124] Elkinani I and Villain J 1993 *Solid State Commun.* **87** 105–8
[125] Krug J, Politi P and Michely T 2000 *Phys. Rev.* B **61** 14037–46
[126] Krug J 2000 *Eur. Phys. J.* B **18** 713–9
[127] Rottler J and Maass P 1999 *Phys. Rev. Lett.* **83** 3490–3
[128] Heinrichs S, Rottler J and Maass P 2000 *Phys. Rev.* B **62** 8338–59
[129] Zorba S, Shapir Y and Gao Y 2006 *Phys. Rev.* B **74** 245410
[130] Politi P 1997 *J. Physique I* **7** 797–806
[131] Kalff M, Šmilauer P, Comsa G and Michely T 1999 *Surf. Sci.* **426** L447–53
[132] Fendrich M and Krug J 2007 *Phys. Rev.* B **76** 121302
[133] Tersoff J, Denier van der Gon A and Tromp R M 1994 *Phys. Rev. Lett.* **72** 266–9
[134] Kandel D 1997 *Phys. Rev. Lett.* **78** 499–502
[135] Teichert C, Hlawacek G, Winkler A, Puschnig P and Ambrosch-Draxl C 2013 Ehrlich–Schwoebel barriers and island nucleation in organic thin film growth *Small Organic Molecules on Surfaces* (*Springer Series in Materials Science*) ed H Sitter, C Ambrosch-Draxl and M G Ramsey (Berlin: Springer) chapter 4, pp 79–106
[136] Quochi F, Andreev A, Cordella F, Orrù R, Mura A, Bongiovanni G, Hoppe H, Sitter H and Sariciftci N S 2005 *J. Lumin.* **112** 321–4
[137] Balzer F and Rubahn H G 2005 *Adv. Funct. Mater.* **15** 17–24
[138] Simbrunner C, Nabok D, Hernandez-Sosa G, Oehzelt M, Djuric T, Resel R, Romaner L, Puschnig P, Ambrosch-Draxl C, Salzmann I, Schwabegger G, Watzinger I and Sitter H 2011 *J. Am. Chem. Soc.* **133** 3056–62
[139] Andreev A, Teichert C, Hlawacek G, Hoppe H, Resel R, Smilgies D M, Sitter H and Sariciftci N S 2004 *Org. Electron.* **5** 23–7
[140] Tumbek L, Gleichweit C, Zojer K and Winkler A 2012 *Phys. Rev.* B **86** 085402
[141] Diebold U 2003 *Surf. Sci. Rep.* **48** 53–229
[142] Hlawacek G, Teichert C, Andreev A, Sitter H, Berkebile S, Koller G, Ramsey M G and Resel R 2005 *Phys. Status Solidi* a **202** 2376–85
[143] Koller G, Berkebile S, Krenn J R, Tzvetkov G, Hlawacek G, Lengyel O, Netzer F P, Teichert C, Resel R and Ramsey M G 2004 *Adv. Mater.* **16** 2159–62
[144] Resel R, Oehzelt M, Lengyel O, Haber T, Schülli T, Thierry A, Hlawacek G, Teichert C, Berkebile S, Koller G and Ramsey M G 2006 *Surf. Sci.* **600** 4645–9

[145] Berkebile S, Koller G, Hlawacek G, Teichert C, Netzer F P and Ramsey M G 2006 *Surf. Sci.* **600** L313–7
[146] Sun L, Berkebile S, Weidlinger G, Koller G, Hohage M, Netzer F P, Ramsey M G and Zeppenfeld P 2010 *Phys. Chem. Chem. Phys.* **12** 3141–4
[147] Söhnchen S, Lukas S and Witte G 2004 *J. Chem. Phys.* **121** 525–34
[148] Madsen M, Kjelstrup-Hansen J and Rubahn H G 2009 *Nanotechnology* **20** 115601
[149] Wu Y, Toccoli T, Zhang J, Koch N, Iacob E, Pallaoro A, Iannotta S and Rudolf P 2009 *Appl. Phys.* A **95** 21–7
[150] Zhang X, Barrena E, de Oteyza D G and Dosch H 2007 *Surf. Sci.* **601** 2420–5
[151] Hlawacek G, Khokhar F S, van Gastel R, Poelsema B and Teichert C 2011 *Nano Lett.* **11** 333–7
[152] Lu W, Soukiassian P and Boeckl J 2012 *MRS Bull.* **37** 1119–24
[153] Hlawacek G, Khokhar F S, van Gastel R, Zandvliet H J W, Poelsema B and Teichert C 2013 *In situ* observation of organic thin film growth on graphene *Small Organic Molecules on Surfaces* (*Springer Series in Materials Science*) ed H Sitter, C Ambrosch-Draxl and M G Ramsey (Berlin: Springer) chapter 5, pp 107–39
[154] Geim A K and Novoselov K S 2007 *Nature Mater.* **6** 183–91
[155] Echtermeyer T J, Lemme M C, Baus M, Szafranek B N, Geim A K and Kurz H 2008 *IEEE Electron. Device Lett.* **29** 952–4
[156] Wang Q H and Hersam M C 2009 *Nature Chem.* **1** 206–11
[157] Lauffer P, Emtsev K V, Graupner R, Seyller T and Ley L 2008 *Phys. Status Solidi* b **245** 2064–7
[158] Wang Z H, Kanai K, Iketaki K, Ouchi Y and Seki K 2008 *Thin Solid Films* **516** 2711–5
[159] Puschnig P 2008 private communication